Agricultural and Forest Meteorology 295 (2020) 108167

Contents lists available at ScienceDirect

Agricultural and Forest Meteorology

journal homepage: www.elsevier.com/locate/agrformet

Hydrometeorological sensitivities of net ecosystem carbon dioxide and methane exchange of an Amazonian palm swamp peatland

T.J. Griffis[a,*], D.T. Roman[b], J.D. Wood[c], J. Deventer[a,d], L. Fachin[e], J. Rengifo[e], D. Del Castillo[e], E. Lilleskov[f], R. Kolka[b], R.A. Chimner[g], J. del Aguila-Pasquel[e], C. Wayson[h], K. Hergoualc'h[i], J.M. Baker[j], H. Cadillo-Quiroz[k], D.M. Ricciuto[l]

[a] Department of Soil, Water, and Climate, University of Minnesota, Saint Paul, MN, USA
[b] USDA Forest Service – Northern Research Station Grand Rapids, MN, USA
[c] School of Natural Resources, University of Missouri, Columbia, MO, USA
[d] University of Goettingen, Bioclimatology, Goettingen, Germany
[e] Instituto de Investigaciones de la Amazonia Peruana, Iquitos, Peru
[f] USDA Forest Service, Houghton, Michigan, USA
[g] Michigan Technological University, Houghton, Michigan, USA
[h] USDA Forest Service, International Programs, Washington, D.C., USA
[i] Center for International Forest Research, Jalan, Situgede, Indonesia
[j] USDA-ARS and University of Minnesota, Saint Paul, MN, USA
[k] Arizona State University, Tempe, AZ, USA
[l] Oak Ridge National Lab, TN, USA

ARTICLE INFO

Keywords:
Methane
Carbon dioxide
Palm swamp
Amazonian peatland
Eddy covariance
Climate change

ABSTRACT

Tropical peatlands are a major, but understudied, biophysical feedback factor on the atmospheric greenhouse effect. The largest expanses of tropical peatlands are located in lowland areas of Southeast Asia and the Amazon basin. The Loreto Region of Amazonian Peru contains ~63,000 km^2 of peatlands. However, little is known about the biogeochemistry of these peatlands, and in particular, the cycling of carbon dioxide (CO_2) and methane (CH_4), and their responses to hydrometeorological forcings. To address these knowledge gaps, we established an eddy covariance (EC) flux tower in a natural palm (*Mauritia flexuosa* L.f.) swamp peatland near Iquitos, Peru. Here, we report ecosystem-scale CO_2 and CH_4 flux observations for this Amazonian palm swamp peatland over a two-year period in relation to hydrometeorological forcings. Seasonal and short-term variations in hydrometeorological forcing had a strong effect on CO_2 and CH_4 fluxes. High air temperature and vapor pressure deficit (VPD) exerted an important limitation on photosynthesis during the dry season, while latent heat flux appeared to be insensitive to these climate drivers. Evidence from light-response analyses and flux partitioning support that photosynthetic activity was downregulated during dry conditions, while ecosystem respiration (RE) was either inhibited or enhanced depending on water table position. The cumulative net ecosystem CO_2 exchange indicated that the peatland was a significant CO_2 sink ranging from -465 (-279 to -651) g C m^{-2} y^{-1} in 2018 to -462 (-277 to -647) g C m^{-2} y^{-1} in 2019. The forest was a CH_4 source of 22 (20 to 24) g C m^{-2} y^{-1}, similar in magnitude to other tropical peatlands and larger than boreal and arctic peatlands. Thus, the annual carbon budget of this Amazonian palm swamp peatland appears to be a major carbon sink under current hydrometeorological conditions.

1. Introduction

Tropical peatlands are long-term carbon dioxide (CO_2) sinks, representing about 88.6 Pg of soil carbon or nearly 20% of global peat carbon (Leifeld and Menichetti, 2018; Page et al., 2011). However, they are also a methane (CH_4) source (Frankenberg et al., 2005; Pangala et al., 2017; Saunois et al., 2017), representing an important biophysical feedback on Earth's radiative forcing (Kirschke et al., 2013). Furthermore, when they are disturbed, and especially when drained for agriculture, they can become a major CO_2 source (Lilleskov et al., 2019). It is important, therefore, to understand the role that intact tropical peatlands play in terms of their net biogeochemical forcing on

* Corresponding author.
E-mail address: timgriffis@umn.edu (T.J. Griffis).

https://doi.org/10.1016/j.agrformet.2020.108167
Received 20 April 2020; Received in revised form 28 July 2020; Accepted 26 August 2020
Available online 11 September 2020
0168-1923/

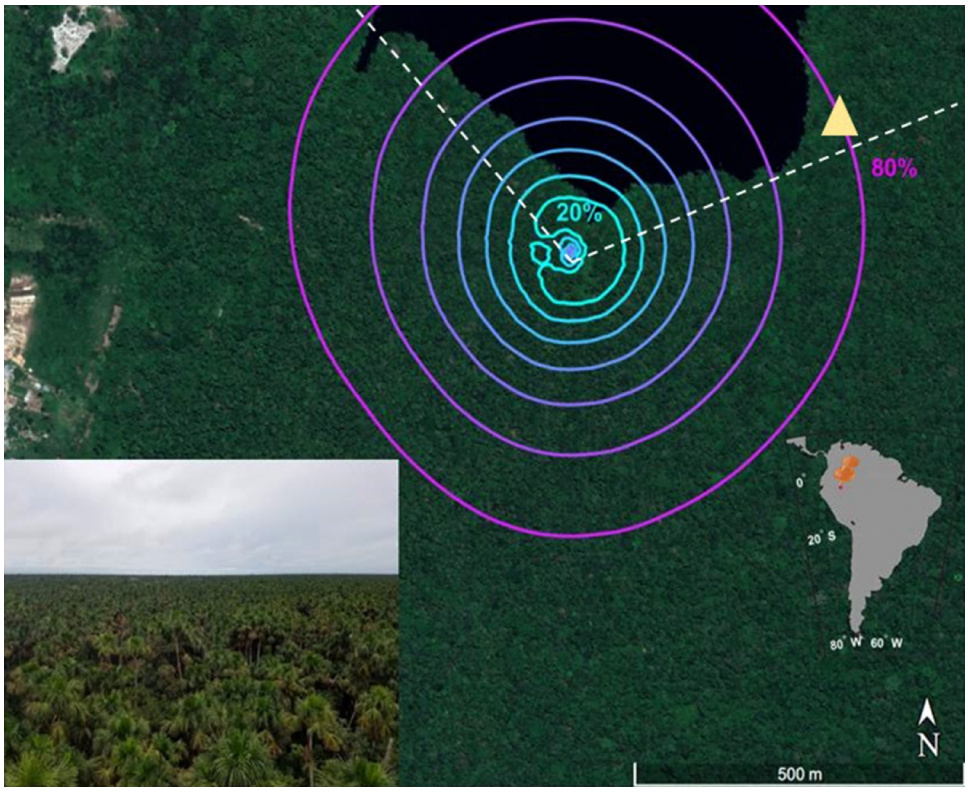

Fig. 1. Research site location and eddy covariance tower flux footprint climatology. The flux footprint was estimated using the model of Kljun et al. (2015). The isopleths indicate the cumulative probability of particle contribution to the total flux. The dashed lines indicate the wind sector that was used to filter out the influence of the lake on the tower flux measurements. The yellow triangle indicates an area of moderate ecosystem disturbance caused by palm fruit harvesting.

climate.

There is evidence for an increase in global CH_4 mixing ratios (i.e. 6.7 ppb/year from 2009 to 2013 and 7.5 ppb/year from 2014 to 2017) with a pronounced increase in equatorial zones (Nisbet et al., 2016; Nisbet et al., 2019). Global top-down and ^{13}C isotope analyses suggest that this increasing trend has largely been driven by changes in natural biogenic sources in response to warmer and wetter tropical conditions (Nisbet et al., 2016; Saunois et al., 2017). However, large uncertainties persist in these source estimates because of a lack of CH_4 observations in the tropics (Knox et al., 2019; Saunois et al., 2020, 2017), and it is difficult to rule out other factors such as increased anthropogenic emissions or decreased CH_4 sink strength (Montzka et al., 2011; Schaefer et al., 2016).

The CO_2 budgets for Amazonian forests have been reported to range from large sinks (Grace et al., 1995; Hutyra et al., 2007; Kiew et al., 2018; Malhi et al., 1998) to large sources (Hutyra et al., 2007; Saleska et al., 2003) depending on forest type, disturbance history, climate, and methodological approaches related to eddy covariance (EC) data filtering and gap-filling. Some key patterns that have emerged indicate that the net uptake of CO_2 can either increase or decrease during the dry ("greening") season (Hutyra et al., 2007; Malhi et al., 1998; Restrepo-Coupe et al., 2013) and that some systems can switch to an annual source resulting from increased ecosystem respiration (RE) during the wet season (Saleska et al., 2003). The majority of these previous studies have examined the CO_2 budgets of evergreen forests growing on mineral soils. To our knowledge, there have been no EC-based studies that have examined the CO_2 or CH_4 budget of palm swamp peatlands, or any peatland, within the Amazonian basin. There is an important need, therefore, for increasing capacity for direct CO_2 and CH_4 flux observations to improve process understanding and to reduce the uncertainties of CO_2 and CH_4 budgets in Amazonian peatlands. Quantifying and understanding the energy balance characteristics of these systems is also needed to help diagnose and model how hydrometeorological forcings influence their carbon budgets.

The largest expanses of tropical peatlands are located in lowland areas of Southeast Asia, the Congo Basin, and the Amazon basin (Dargie et al., 2017; Gumbricht et al., 2017; Page et al., 2011). The Loreto Region of Amazonian Peru is comprised of about 63,000 km^2 of peatlands within the Pastaza-Marañon Foreland Basin (PMFB) (Draper et al., 2014). However, the extent of low elevation peatlands in Peru has only recently been documented, and little is known about their biogeochemistry and ecophysiology. To help address these knowledge gaps, we established an EC flux tower in a low disturbance palm swamp peatland in the Quistococha Forest Park (AmeriFlux Site PE-QFR, https://ameriflux.lbl.gov/sites/siteinfo/PE-QFR), near Iquitos, Peru in spring 2017 in collaboration with the Instituto de Investigaciones de la Amazonia Peruana (IIAP). The objectives of this current research were to: 1) Present the first measurements of energy fluxes and net ecosystem CO_2 and CH_4 exchange from an Amazonian palm swamp peatland; 2) Examine how the biophysical controls and magnitudes of these fluxes differ from other Amazonian forests; and 3) Assess if these ecosystems have a net radiative cooling effect on climate when considering the contemporary CO_2 and CH_4 balance and global warming potentials (GWP).

2. Methodology

2.1. Research site

The study site is located in the equatorial Amazon in a natural protected forest park named Quistococha, 10 km southwest of Iquitos city in the Loreto Region of Peru. The park is administrated by the Office of Tourism of the Regional Government (DIRCERTUR) and is an official scientific research area for IIAP. The EC flux tower (42 m) is located at 73° 19′ 08.1" W; 3° 50′ 03.9" S, and 104 m above sea level, within a natural low disturbance palm swamp peatland that is part of the park. The tower location and the flux footprint climatology (Kljun et al., 2015) are shown in Fig. 1. We note that fetch is inadequate for northerly wind flow and these data have been filtered according to quality control assessments (described below). The flux footprint generally represents a pristine natural tropical peatland, but does include some potential influence where forest degradation is taking place

(Fig. 1). Bhomia et al. (2019) have quantified some areas of disturbance near the site as medium impact. Here, *Mauritia flexuosa* have been cut for their fruits and woody trees have been cleared, leading to differences in forest structure and composition compared to the pristine areas. Two disturbance areas have been well documented in the Bhomia et al. (2019) study. First, there is a disturbed area located approximately 1 km SSW of the tower and more than 400 m from the flux footprint 80% isopleth. Second, there is an area of disturbance located NE of the tower, which is adjacent to the lake and, consequently, has been filtered according to our flux footprint QA/QC procedures.

Palaeoecological studies indicate that peat began to form at this site about 2200 to 2300 years before present (BP), and the current vegetation community was established about 400 years BP (Roucoux et al., 2013). The tree density and basal area for the study site is approximately 1846 ± 335 trees ha^{-1} and 19.4 ± 2.8 m^2 ha^{-1}, respectively for stems with diameter at breast height (DBH) greater than 10 cm (Bhomia et al., 2019). The major palm type, ranked by stem density and basal area, is *Mauritia flexuosa* L.f. (21.3 m height on average), which represents about 65% of the total palm basal area at this site (Bhomia et al., 2019; Roucoux et al., 2013). The next most important tree species within Quistococha, ranked according to stem density, include *Tabebuia insignis, Hevea nitida, Mauritiella armata*, and *Fabaceae* sp. (Bhomia et al., 2019; Roucoux et al., 2013). The peatlands in the Quistocochia study area range from oligotrophic to minerotrophic because they are seasonally or intermittently inundated by floodwater from the major rivers (*Draper et al.* 2014; Lähteenoja et al., 2009a; Finn et al., 2020). Total aboveground and belowground biomass carbon stocks are estimated at 97.7 ± 15 Mg C ha^{-1} and 24.9 ± 4.1 Mg C ha^{-1}, respectively (Bhomia et al., 2019). The vegetation at this site is broadly representative of the Pastaza-Marañon basin, where *M. flexuosa* is the dominant palm species, and is under significant anthropogenic pressure within the region for its valuable source of fruits, with destructive harvest reducing population density in unprotected forests (Hergoualc'h et al., 2017).

The peat layer thickness varies from 1.92–2.45 m (Bhomia et al., 2019; Lähteenoja et al., 2009b) with a total soil C pool of ~740 Mg C ha^{-1}. Overall, the average ecosystem carbon stock, including soil, litter, debris, and vegetation, for Quistococha is approximately 876.9 ± 108.5 Mg C ha^{-1} (Bhomia et al., 2019). The historical average soil carbon accumulation for these peatlands, estimated from peat inventories and carbon dating, is approximately 74 ± 15 g C m^{-2} y^{-1} over the past 2300 years (Lähteenoja et al., 2009b).

The mean annual air temperature and precipitation for the Puerto Almendras Ordinary Weather Station (6 km from the EC tower site), Iquitos (2003–2017) were 27.2 °C and 2753.2 mm, respectively (Servicio Nacional de Meteorología e Hidrología del Perú, 2019). The site is characterized by a wet season (typically February to April) with minimum and maximum air temperatures of 22.9 °C and 31.8 °C, respectively, and a dry season (typically August to September) with minimum and maximum air temperature of 22.5 °C and 32.7 °C, respectively. Precipitation during the wet and dry seasons is typically 810 mm and 545 mm, respectively. The water table position is often located above the soil surface during the latter part of the wet season (i.e. 80 to 150 cm in May and June) and rarely drops below a level of 20 cm from the soil surface (Hergoualc'h et al., 2020; Kelly et al., 2017). Although the site is characterized by a dry season (reduced precipitation) we note that during this study that soil water availability was non-limiting.

2.2. Micrometeorological measurements

Eddy covariance flux measurements of energy, water vapor, CO_2 and CH_4 were established in January 2017. However, CH_4 flux measurements during 2017 and 2018 were made sporadically due to sensor failure related to a manufacturer defect. Furthermore, a lightning strike in early 2017 caused substantial damage to the instrumentation and major data loss. Consequently, we focus our analyses on the period January 1, 2018 to December 31, 2019 for energy and CO_2 fluxes and January 1, 2019 to December 31, 2019 for CH_4 fluxes.

The EC system consists of open-path analyzers for CH_4 (LI-7700, LI-COR Inc., Lincoln, NE, USA) and CO_2 (LI-7500, LI-COR Inc.) with turbulence measured using a 3D ultrasonic anemometer (CSAT3, Campbell Scientific Inc. Logan, UT, USA) mounted at 40 m above the ground (about 20 m above the mean canopy height). In February 2019, a new LI-7700 was installed at the site to improve the reliability of the CH_4 flux measurements. A datalogger (CR5000, Campbell Scientific Inc., Logan UT, USA) was used to record data from the EC sensors that were sampled at a rate of 10 Hz. Our group has tested and evaluated the long-term (3.5 years) performance of the LI-7700 analyzer in comparison to a closed-path system (TGA100A, Campbell Scientific Inc.) at a subboreal peatland site (Deventer et al., 2019), and found good agreement in half-hourly fluxes and excellent agreement on annual budgets. Here, we apply the same flux processing strategies performed by Deventer et al. (2019).

Raw 10 Hz data were processed and block-averaged to half-hourly fluxes using the EC approach (Baldocchi et al., 1988). We used custom software developed in MATLAB (The Mathworks Inc., Natick, MA, USA) for raw data processing and flux calculations (Deventer et al., 2019; Wood et al., 2017) and followed the recent ICOS (Integrated Carbon Observation System) guidelines for CO_2 and H_2O flux calculations (Sabbatini et al., 2018) and CH_4 flux calculations (Nemitz et al., 2018). Raw data quality checks included completeness of the dataset, amplitude resolution, and dropouts. Further, the raw data (not including CH_4) were de-spiked and time lags between wind velocity and scalar measurements were compensated for by maximizing the covariance. Spectral corrections for high-pass (Moncrieff et al., 2006) and low-pass (Fratini et al., 2012) filtering and lateral sensor separation (Horst and Lenschow, 2009) were applied. Half-hour wind vectors and fluxes were rotated into the natural wind coordinate system using a two-dimensional rotation (Tanner and Thurtell, 1969; Morgenstern et al., 2004). The Webb-Pearman-Leuning (WPL) terms were applied to compensate for the effects of sensible (*H*) and latent heat (*LE*) fluxes on measured CO_2 and CH_4 density fluctuations (Webb et al., 1980). Spectroscopic corrections were also applied to the CH_4 open-path measurements (McDermitt et al., 2011). A correction associated with sensor-path heat exchange (i.e. 'sensor self-heating') of the CO_2/H_2O open-path analyzer was computed following Burba et al. (2008). A single-level storage flux term was calculated and summed with the turbulent fluxes to estimate net ecosystem exchange of energy, CO_2 and CH_4 following Morgenstern et al. (2004) (Fig. S1). We observed very similar diel patterns of storage to that described in Morgenstern et al. (2004) and a similar ratio of storage flux to eddy flux for CO_2.

Flux QA/QC was based on sensor diagnostics, wind direction, as well as low friction velocity (u_*). Periods of sensor malfunction were identified by sensor diagnostic values, as well as low signal strength of the open-path gas analyzers (RSSI < 10 for LI-7700, and AGC > 90 for the LI-7500). A wind direction filter (WD > 320° or WD < 70°) was applied to eliminate periods when the flux footprint was influenced by the nearby lake. Periods of low u_* were removed by applying an annual threshold ($u_* = 0.082$ m s^{-1}) that was determined using the REddyProc package, which implemented the moving point detection method (Papale et al., 2006). After applying these QA/QC procedures, the time series of half-hourly fluxes for net ecosystem CO_2 exchange (CO_2 NEE), *LE* and *H* were de-spiked following the methods of Papale et al. (2006), while the CH_4 flux (NEE CH_4) time series was filtered following Taylor et al. (2018) by removing any points outside of 2 standard deviations of the overall mean.

Following these QA/QC procedures, the data retention was approximately 28% and 44% for energy, 23% and 36% for CO_2, and 0% and 26% for CH_4 in 2018 and 2019, respectively. The 0% retention in 2018 for CH_4 was caused by sensor failure.

Gap-filling of CO_2 fluxes was performed to estimate annual budgets following the look-up table method based on the approach of

Reichstein et al. (2005) and were implemented in the REddyProc package. The uncertainty in the annual totals resulting from data losses and gap-filling was determined using a Monte-Carlo strategy (Griffis et al., 2003). Here, we artificially increased the amount of missing observations by randomly removing 5%, 10%, 15%, and 20% of the valid data and repeated this process 500 times per year. The uncertainty in cumulative NEE increased from about 13% to 40% as we increased data loss from 5% to 20%, respectively. We also observed a slight increase in the cumulative carbon uptake as a function of the amount of missing data (Fig. S2 and Table S1).

We provide CO_2 NEE budget estimates with and without the sensor self-heating corrections applied because there is considerable debate regarding its application (Deventer et al., 2020). The annual CH_4 NEE budget was estimated using two approaches: 1) by fitting a skewed Laplace distribution to the half-hourly observations for each month and then extrapolating these monthly mean fluxes to an annual budget; and 2) by using an artificial neural network (ANN) modeling approach to replace missing or invalid observations following Deventer et al. (2019).

The partitioning of CO_2 NEE into gross primary productivity (GPP) and ecosystem respiration (RE) was performed using the REddyProc package (Wutzler et al., 2018). Here we use the micrometeorological sign convention for NEE (i.e. a negative flux indicates a net ecosystem sink) where NEE = RE – GPP. The REddyProc package employs the Lasslop et al. (2010) approach, which utilizes a hyperbolic light-response curve to model RE from the daytime CO_2 NEE data (Falge et al., 2001). This algorithm accounts for vapor pressure deficit (VPD) limitation on photosynthesis following (Körner, 1995) and uses modeled RE to account for the temperature dependency of respiration (Lloyd and Taylor, 1994).

Supporting hydrometeorological measurements included net radiation (NR-lite, Kipp and Zonen, B.V., Delft, The Netherlands), solar radiation (LI-200R, LI-COR Inc.), photosynthetically active radiation (LI-190R, LI-COR, Inc.), air temperature and relative humidity (HMP45C, Campbell Scientific Inc.), precipitation (TE-525L, Texas Electronics Dallas, TX, USA), soil volumetric water content (CS616, Campbell Scientific Inc.), measured at a soil depth of 10 cm and soil heat flux (HFP01-L, Hukseflux Inc., Delft, Netherlands) measured at a soil depth of 10 cm. Water table position was measured using a HOBO-U20 water level data logger (Onset Computer Corporation, Bourne, MA, USA), which was deployed 1 m below the soil surface within a plot 500 meters northwest of the tower.

3. Results and discussion

3.1. Hydrometeorology and phenology

A distinguishing hydrometeorological feature between 2018 and 2019 was the duration and intensity of the dry season (Fig. 2). In 2018, the dry season was characterized by monthly precipitation totals less than 140 mm over the period June through October. In 2019, the dry season was limited in duration to August through September. Total precipitation in 2018 was 3032.9 mm (10.2 mm/d and 4.4 mm/d for the wet and dry seasons, respectively) and 2943.9 mm in 2019 (10.1 mm/d and 3.5 mm/d for the wet and dry seasons, respectively), which exceeded the average for the most recent 15-year period (2003 to 2017) at Iquitos. This site is characterized by a stable thermal environment at seasonal to annual time scales. The mean annual air temperatures in 2018 and 2019 were 25.6 °C and 25.7 °C, respectively. The mean seasonal peak-to-trough amplitude of daily average air temperature was approximately 1.5 °C (Fig. 2). During the wet and dry seasons, the mean air temperatures were remarkably similar at 26.0 °C and 26.1 °C and 25.6 °C and 26.2 °C for 2018 and 2019, respectively. The mean annual air temperature in both years was about 1.5 °C lower compared to the recent 15-year period for Iquitos.

Leaf area index (LAI) from the Moderate Resolution Imaging Spectroradiometer (MODIS, MCD15A2H Version 6) (ORNL DAAC, 2018; Myneni et al., 2015) showed seasonality that followed wet/dry season patterns (Figs. 3 and S3). The mean annual LAI (± 1 standard deviation) in 2018 and 2019 was 3.9 (± 0.8) and 4.90 (± 0.8), respectively, which is slightly lower than the 5-year mean LAI of 4.1 (± 0.5). Note that some of the short-term variability in LAI is likely caused by the effects of weather conditions on the MODIS LAI retrieval. LAI typically reached 4 to 5 at the end of the wet period (around day of year, DOY, 100), with a pronounced seasonal peak of about 5 during the dry period (~DOY 250). The mean LAI during the 2018 wet and dry seasons was 3.2 ± 0.6, 4.4 ± 0.9, respectively; while in 2019, mean wet and dry season LAI was 3.7 ± 0.8, 5.0 ± 0.4, respectively. The higher LAI observed during the dry season was statistically significant ($p < 0.01$) according to a two-sample t-test. Similar patterns, magnitudes, and seasonal amplitudes of LAI have been reported previously in the Amazon and are thought to be driven by net leaf abscission during the wet season followed by net leaf flushing during the dry season (Huete et al., 2006; Myneni et al., 2007; Saleska et al., 2016; Smith et al., 2019).

The mean annual net radiation (R_n) balance in 2018 (110.8 ± 202.8 W m^{-2}) was nearly identical to that in 2019 (111.2 ± 203.5 W m^{-2}) (Fig. 4). The mean midday values of R_n were approximately 450 ± 200 W m^{-2} during the wet season and increased to about 500 ± 202 W m^{-2} during the dry period because of clearer sky conditions. The mean daytime VPD at 41 m height, was 8.0 hPa (8.7 hPa for the wet period; 8.8 hPa for the dry period) and 7.3 hPa (6.8 hPa for the wet period; 10.5 hPa for the dry period) in 2018 and 2019, respectively. In both years, there were instances when VPD increased substantially during the dry period. For example, on DOY 242 (August 30, 2019) air temperature and VPD exceeded 31 °C and 17 hPa, respectively (Fig. 4). Water table position was on average, above the surface in 2018 (+0.034 m) and 2019 (+0.034 m). However, the seasonal dynamics and range varied considerably between each year (Fig. S4). In 2019, the water table position showed slightly more dynamic range (0.35 m) compared to 2018 (0.32 m). In 2018, water table position was relatively low during the early wet season and over the period DOY 170 (June 19) to DOY 290 (October 17). In 2019, the water table was generally at or above the surface, but was periodically below the surface from DOY 215 (August 3) to DOY 330 (November 26). Volumetric soil water content (θ, measurements initiated in 2019) remained above 0.77 in 2019 (Fig. S4). During the dry season, θ showed a steady decline after DOY 150 (May 30) and reached a minimum value on DOY 240 (August 28).

The energy balance closure for this site (Fig. S5) was reasonably good with turbulent heat fluxes ($H + LE$) accounting for more than 72% of the available energy (R_n-S). The energy balance closure at this site was in the range (i.e. 0.53 to 0.99) reported for a broad range of AmeriFlux sites (Wilson et al., 2002) and was similar to the energy balance closure (0.70 to 0.78) reported for broadleaf and wetland sites (Stoy et al., 2013). The dominant sink for the available energy was LE (Fig. 5). On an annual basis, mean midday LE was approximately 255 W m^{-2}, and nearly identical in both years. The median Priestley-Taylor coefficient ($\alpha = 1.12$) indicated that evaporation was not significantly limited by water availability or canopy resistance. Mean midday H flux for the same period was approximately 60 W m^{-2}, yielding midday Bowen ratio ($= H/LE$) values that were typically 0.24. Mean midday LE peaked at about 300 W m^{-2} during the dry season. The midday wet season LE was about 30 to 90 W m^{-2} lower than during the dry season, indicating that LE was energy limited. This is supported by the fact that the mean equilibrium evaporation rate increased from 350 W m^{-2} during the wet season to 400 W m^{-2} during the dry season. As expected, LE was a strong linear function of R_n ($LE = 0.54R_n + 23.7$, $r^2 = 0.76$, RMSE = 54.3, df = 12,602, $p < 0.01$, all data combined for 2018 and 2019) and was relatively insensitive to changes in VPD or air temperature, T_a (Figs. 6 and S6) or water table position. Overall, LE accounted for about 54% of R_n. These Bowen ratio values and evaporative fractions are considerably lower than the first ever

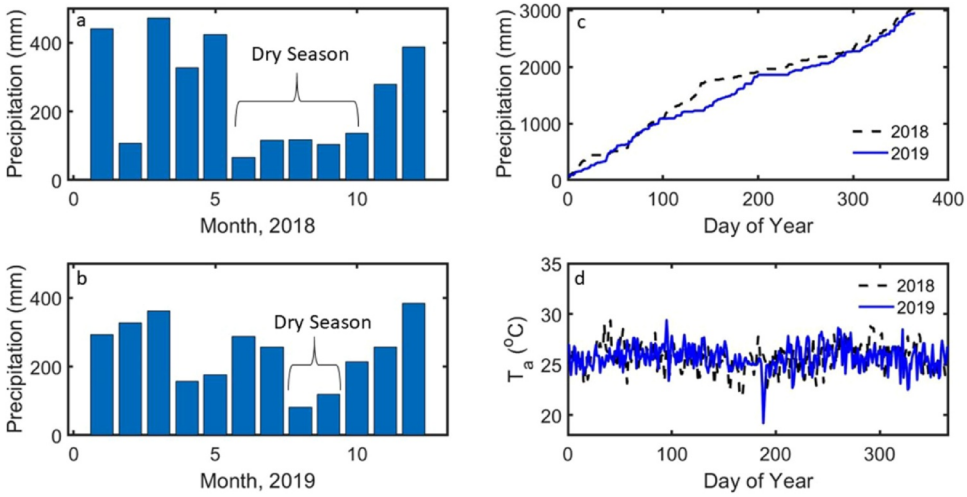

Fig. 2. (a) Monthly total precipitation in 2018; (b) Monthly total precipitation in 2018; (c) Cumulative precipitation in 2018 and 2019; (d) daily average air temperature measured at the flux tower at a height of 40 m.

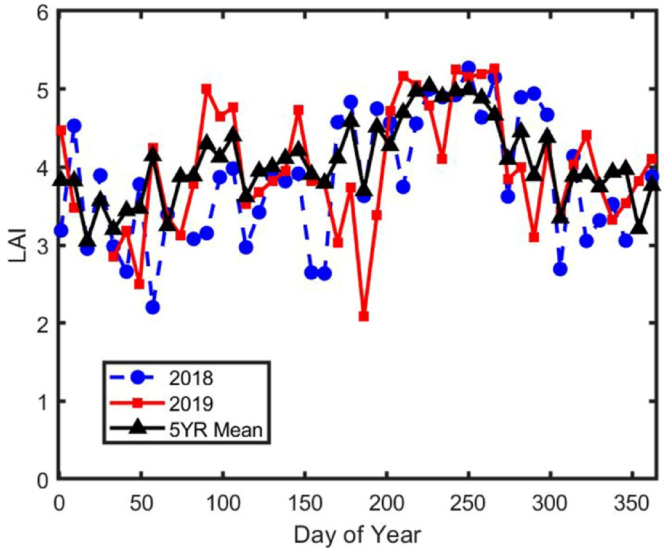

Fig. 3. Leaf area index (LAI) estimated with the MCD15A2H Version 6 Moderate Resolution Imaging Spectroradiometer (MODIS) Level 4.

measurements (Bowen ratio = 0.43 and evaporative fraction = 0.698) reported for a tropical rain forest by Shuttleworth et al. (1984). The cumulative evaporative flux accounted for about 1100 mm or 36% of the annual precipitation. These results imply that runoff and drainage are an important component of the water balance and, therefore, the carbon balance in these palm swamp peatlands (discussed in Section 3.5).

Analyses of energy balance data from the Large Scale Biosphere-Atmosphere Experiment in the Amazon (LBA) also support these findings (da Rocha et al., 2009). Their research demonstrated that "wet" sites, experiencing greater than 1900 mm of annual precipitation, showed higher *LE* during the dry season when available energy increased due to reduced cloud cover. The LBA wet sites showed Bowen ratio values that were in the range of 0.32 to 0.36, indicating that the Quistococha palm swamp forest studied here was wetter with relatively more energy partitioned into *LE* (i.e. Bowen ratio of ~ 0.24). The diel *LE* patterns described here for the wet and dry seasons are consistent with those reported by Hutyra et al. (2007) for a primary growth evergreen forest, located in the Tapajós National Forest, Pará, Brazil. In their study, they concluded that *LE* increased during the dry season and observed a similar linear relation with R_n for the wet and dry seasons (i.e. *LE* was a linear function of R_n with a slope of 0.57 for wet seasons and 0.54 for dry seasons). In contrast, *LE* has been reported to peak during the wet season at other Amazonian sites (Malhi et al., 2002; Vourlitis et al., 2002). Malhi et al. (2002) found that *LE* was limited during the dry season by a reduction in canopy conductance in response to reduced soil water content. They showed that *LE* was a linear function of R_n with a slope of 0.65 during the wet season and a slope of only 0.38 during the dry season. Given the relative high water table position at the Quistococha site (Fig. S4), and the lack of response of *LE* to changes in VPD (Figs. 6 and S6), we conclude that *LE* was not water limited during the dry period of 2018 or 2019. Our results support a broader analysis of energy balance in the tropics that found R_n explained 87% of the variance in monthly *LE* across sites with an evaporative fraction (LE/R_n) of 0.72 (Fisher et al., 2009).

3.2. Net ecosystem CO_2 exchange

Half-hourly CO_2 NEE ranged from about −60 to +30 μmol m^{-2} s^{-1} over the two-year period. The annual mean midday CO_2 NEE was about −20 ± 8 μmol m^{-2} s^{-1} in both years (Fig. 7). In each year, net CO_2 uptake was diminished immediately after the wet season and through the duration of the dry season (Fig. 7) despite higher LAI and greater available energy in the dry season. This seasonal effect was related to a reduction in GPP (described below) and was more pronounced in 2018 because of a more intense dry down that extended from June through October (Fig. 2). The water table position dropped during this period, but remained above the surface (Fig. S4). Similar results have been reported by Kiew et al. (2018) for a peat swamp forest in Sarawak, Malaysia. They concluded that enhanced RE during the dry season was the dominant control on NEE. In contrast, Hutyra et al. (2007) found that phenology and available light were the dominant controls *via* canopy photosynthesis in an evergreen tropical rain forest in Tapajós. Here, we observed a decline in GPP during dry periods and a more variable response in RE (described below).

In 2018, CO_2 NEE reached –26.0 μmol m^{-2} s^{-1} at midday during the wet season, but was substantially lower at −18.2 μmol m^{-2} s^{-1} during the dry season. Similar patterns were observed in 2019, with midday CO_2 NEE reaching −20.6 μmol m^{-2} s^{-1} during the wet season. The dry season midday fluxes were also diminished (−16.0 μmol m^{-2} s^{-1}). The magnitude of peak daytime CO_2 NEE at Quistococha was in very good agreement with that observed for a lowland *terra firme* (mineral soil wetland) tropical rain forest at the Reserva Biológica do Cuieiras, Amazonia, Brazil (Malhi et al., 1998). They observed a mean net uptake of CO_2 at midday of about −15 to −20 μmol m^{-2} s^{-1}. Very

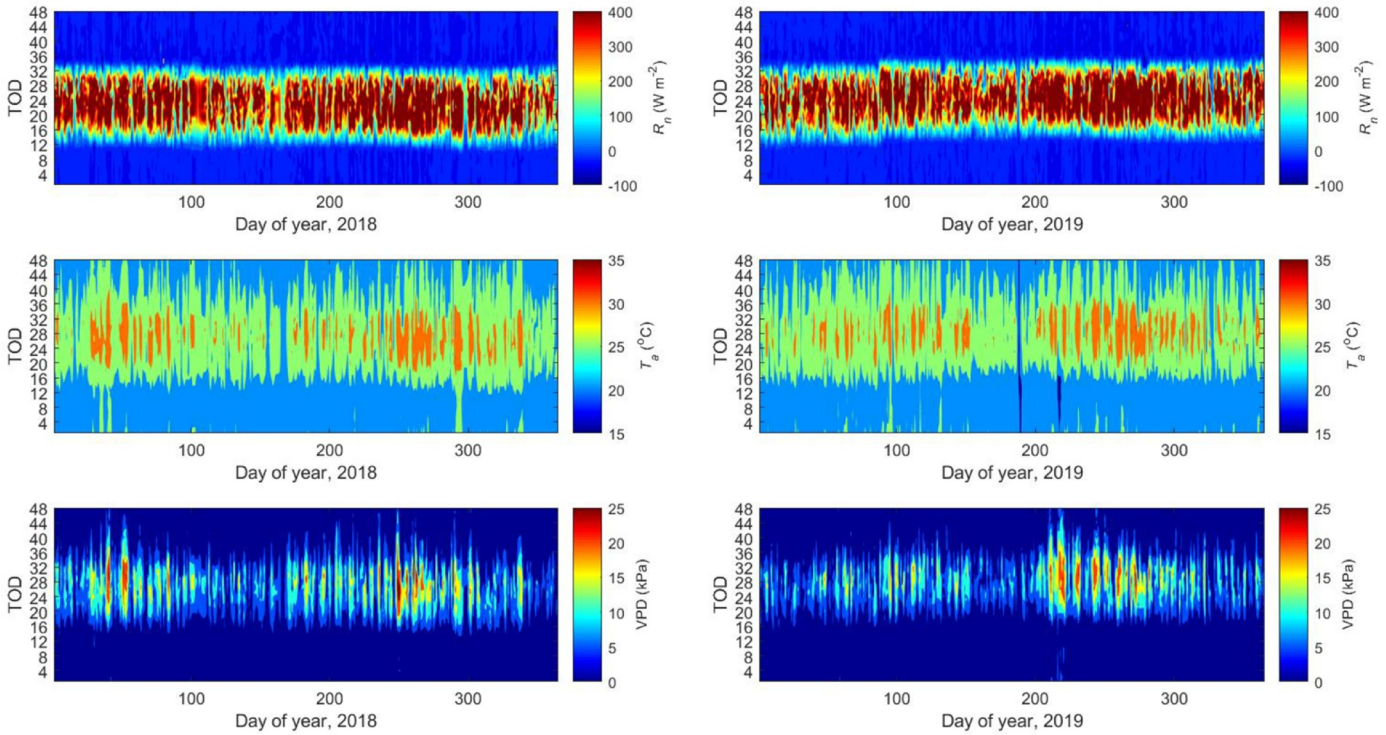

Fig. 4. Flux tower climatology. Upper panels) Half-hourly net radiation values in 2018 and 2019; Middle panels) Half-hourly values of air temperature in 2018 and 2019; Lower panels) Half-hourly values vapor pressure deficit values in 2018 and 2019. The y-axes indicate the time of day (TOD) as half-hourly values.

similar daytime patterns were also reported by Carswell et al. (2002) for a *terra firme* forest near Belém, Pará, Brazil (eastern Amazonia).

We combined data from 2018 and 2019 to examine the light response of CO_2 NEE. The photosynthetic and respiratory parameters were obtained using a non-linear least squares optimization of the light-response function following Landsberg and Gower (1997) and Griffis et al. (2003). These light response analyses indicated a mean apparent canopy photosynthetic capacity (A_{max}), apparent quantum yield (α), and day respiration (R_d) of 43.0 μmol m^{-2} s^{-1}, 0.09, and 11.9 μmol m^{-2} s^{-1}, respectively (Fig. 8 and Table 1). These values are consistent with other tropical rain forests (Malhi et al., 1998) and are similar to that reported for deciduous aspen boreal forests during peak summer growth (Griffis et al., 2003). There was evidence that high values of PAR, air temperature, and VPD limited the uptake of CO_2 in this palm swamp forest (Figs. 8 and S7). Light-response analyses conducted by Malhi et al. (1998) also found evidence of reduced apparent photosynthetic capacity at elevated VPD (see their Fig. 6b). High air temperature and VPD can reduce stomatal conductance, despite having ample soil water because stomatal conductance is largely determined by leaf water status (Buckley, 2019, 2017). If the evaporative demand exceeds what the plant vascular system can supply, the leaf can lose turgor, despite adequate available soil water. Similar patterns have been observed for other wetlands and peatlands (Blanken and Rouse, 1996; Otieno et al., 2012) and more broadly across eddy covariance flux sites (Novick et al., 2016).

Additional light-response analyses were conducted for conditions when the air temperature was above or below a threshold of 25 °C. These analyses indicated a substantial reduction in A_{max} at high temperatures. The light-response parameters for low vs high temperature conditions were A_{max} = 57.8 μmol m^{-2} s^{-1}, α = 0.07, and R_d = 11.6

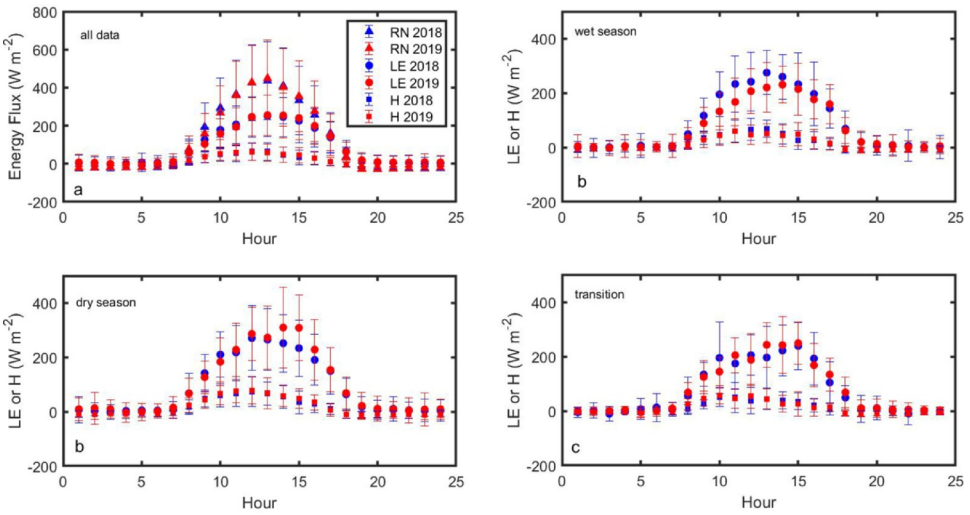

Fig. 5. Energy balance characteristics of the flux tower site. (a) net radiation, latent heat flux and sensible heat flux including all half-hourly values for 2018 and 2019; (b) latent and sensible heat flux during the dry seasons in 2018 and 2019; (c) latent and sensible heat flux during the wet seasons in 2018 and 2019; (d) latent and sensible heat flux during the transition season in 2018 and 2019.

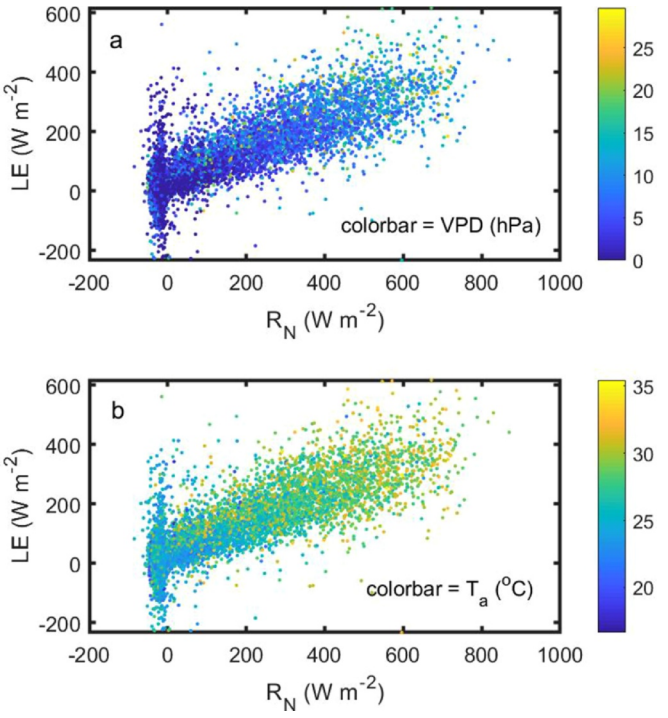

Fig. 6. Evaporative fraction - latent heat flux as a function of net radiation. (a) color bar indicates vapor pressure deficit (hPa); (b) color bar indicates air temperature (°C).

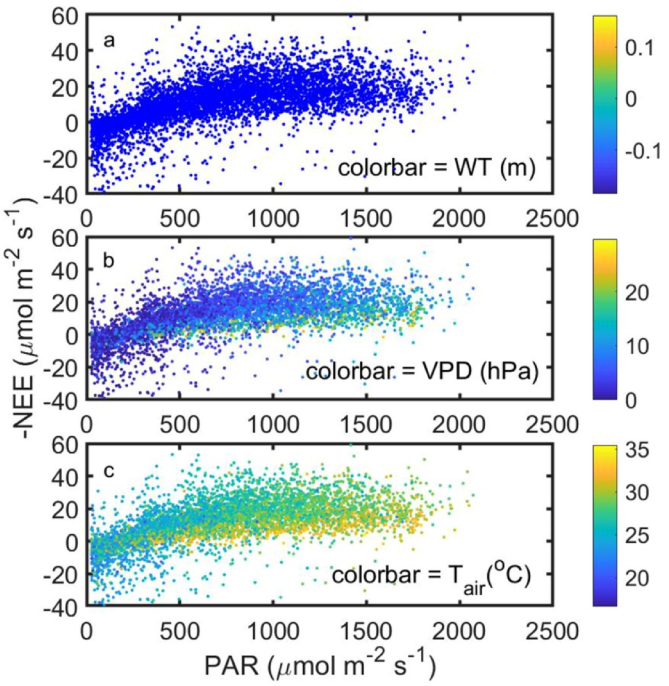

Fig. 8. Canopy scale light-response CO_2 NEE analyses. (a) Combining all available data for 2018 and 2019 where the color bar indicates water table position (m); (b) All data combined where color bar indicates vapor pressure deficit (hPa); (c) All data combined where color bar indicates air temperature (°C). Note that a minimum PAR threshold of 25 μmol m^{-2} s^{-1} was used and that NEE data are plotted as -1 × NEE.

μmol m^{-2} s^{-1} (R^2 = 0.35, *df* = 1176) vs A_{max} = 40.6 μmol m^{-2} s^{-1}, α = 0.09, and R_d = 10.7 μmol m^{-2} s^{-1} (R^2 = 0.39, *df* = 4703), respectively (Table 1).

Light response analyses for the wet and dry seasons indicated substantially higher photosynthetic capacity (A_{max}) during the wet season (Table 1), despite the differences observed in LAI. During the 2018 wet season, the A_{max} was 58.0 μmol m^{-2} s^{-1} versus 37.7 μmol m^{-2} s^{-1} during the dry season (Fig. 9). A less pronounced pattern was observed in 2019, with a wet season A_{max} of 45.5 μmol m^{-2} s^{-1} and a dry season A_{max} of 40.0 μmol m^{-2} s^{-1}. Our analyses indicated that higher PAR and VPD and lower water table position during the dry seasons limited photosynthesis. For example, in 2018 mean PAR, VPD, and WT values were +20 μmol m^{-2} s^{-1}, +1.0 hPa, and -1.2 cm, relative to the wet season values. These analyses also suggest that the higher available energy during the dry season enhanced surface evaporation relative to plant transpiration.

We found that mean annual midday GPP was about 26.0 ± 8.1 μmol m^{-2} s^{-1} and midday RE was approximately 8.1 ± 7.9 μmol m^{-2} s^{-1} (Figs. 10 and 11). The partitioned GPP values showed evidence for light-inhibition at PAR values greater 1000 μmol m^{-2} s^{-1} and limitation imposed by high air temperature and VPD (Fig. S7). There was also some evidence for declining GPP associated with the interplay between low water table position and high VPD (Fig. S7). During the 2018 dry season, GPP was substantially reduced (i.e. by 8 μmol m^{-2} s^{-1}) compared to the wet season, while midday partitioned RE decreased by

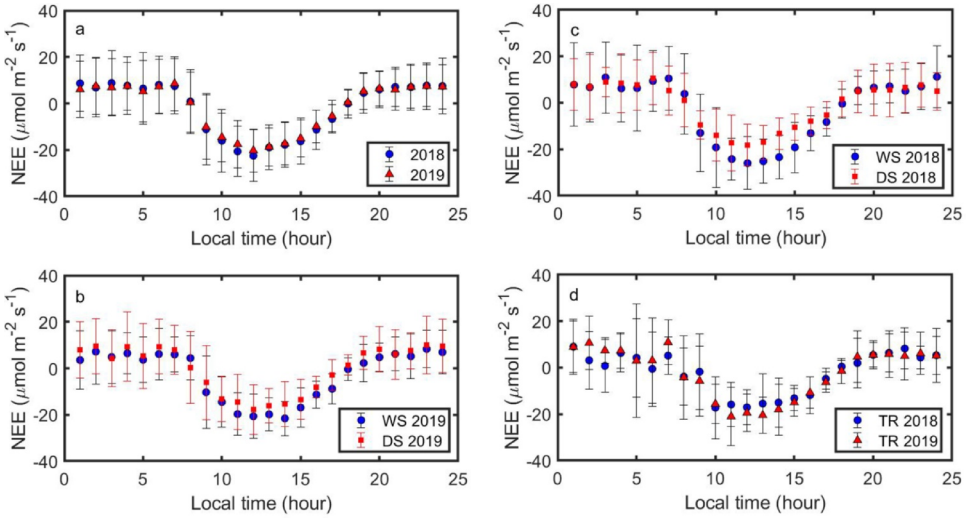

Fig. 7. Diel patterns of net ecosystem CO_2 exchange. (a) all data; (b) wet season and dry season in 2018; (c) wet season and dry season in 2019; (d) transition season in 2018 and 2019.

Table 1
Summary of canopy-scale light-response analyses.

Data Selection	A_{max} (μmol m^{-2} s^{-1})	Alpha (unitless)	R_d (μmol m^{-2} s^{-1})	Fit
All data	43.0 (41.7 to 44.4)	0.09 (0.08 to 0.11)	11.9 (10.6 to 13.2)	R^2 = 0.44; df = 5882
T_{air} < 25 °C	57.8 (44.0 to 71.5)	0.07 (0.05 to 0.09)	11.6 (9.6 to 13.7)	R^2 = 0.35; df = 1176
T_{air} > 25 °C	40.6 (39.1 to 42.1)	0.09 (0.07 to 0.11)	10.7 (8.9 to 12.4)	R^2 = 0.39; df = 4703
Wet 2018	58.0 (52.0 to 64.0)	0.10 (0.07 to 0.14)	13.5 (9.4 to 17.6)	R^2 = 0.51; df = 616
Dry 2018	37.8 (33.8 to 41.7)	0.06 (0.04 to 0.08)	9.2 (6.4 to 12.0)	R^2 = 0.41; df = 797
Wet 2019	45.5 (41.9 to 49.1)	0.09 (0.06 to 0.12)	10.7 (7.8 to 13.7)	R^2 = 0.51; df = 820
Dry 2019	40.0 (34.4 to 45.7)	0.06 (0.03 to 0.08)	10.6 (6.9 to 14.3)	R^2 = 0.38; df = 637

*numbers in parentheses indicate the 95% confidence intervals (lower, upper)

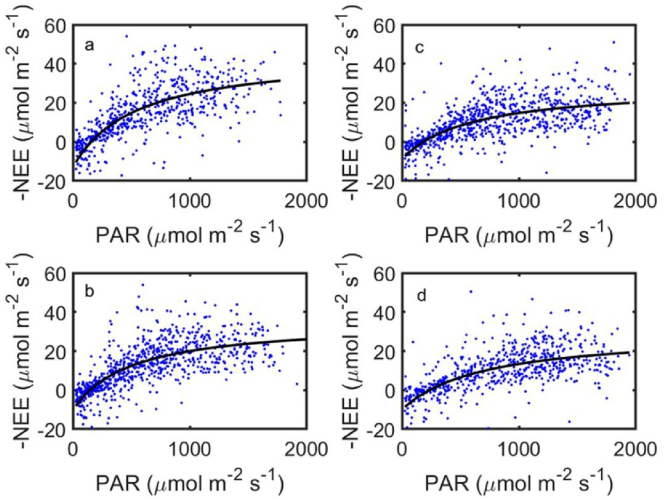

Fig. 9. Canopy scale light-response CO_2 NEE analyses for the dry and wet seasons in 2018 and 2019. (a) wet season 2018; (b) dry season 2018; (c) wet season 2019; (d) dry season 2019. Note that a minimum PAR threshold of 25 μmol m^{-2} s^{-1} was used and that NEE data are plotted as -1 × NEE.

about 2 μmol m^{-2} s^{-1}. These results are somewhat surprising given the relatively high water table position and soil water content observed over the entire year. Such sensitivity to drier conditions (Fig. S7) suggests that a substantial decline in the carbon sink strength could occur as air temperature continues to warm (Gloor et al., 2018) in the tropics or if the frequency of El Niño events or warm tropical North Atlantic Sea Surface Temperature (NTA-SST) anomalies increase (discussed further in Section 3.5). This hydrometeorological sensitivity highlights the need for longer-term measurements in these systems to assess the potential for acclimation and longer-term feedback responses.

The patterns we observed at this equatorial Amazonian site differed from LBA sites (Restrepo-Coupe et al., 2013; Saleska et al., 2003). For instance, Restrepo-Coupe et al. (2013) found that the dry season caused an increase in LAI and a progressive increase in canopy photosynthetic capacity at their equatorial flux site. Saleska et al. (2003) concluded that variations of RE was the dominant control on seasonal CO_2 NEE dynamics. They observed significant increases in RE during the wet season that contributed to a net carbon source in some years. Our results imply that RE is suppressed by flooding and likely redox limited. Recent work at a flood plain Amazonian forest near Cantão State Park, Brazil demonstrated that ecosystem productivity was limited by excessive soil water content during the flooded season, while GPP was enhanced by higher soil water content values during the dry/non-flooded period (Fonseca et al., 2019). Koren et al. (2018) reported a significant reduction in SIF, a proxy for GPP, for the western (2 to 5%) and eastern (10 to 15%) Amazon Basin, associated with high air temperatures and reduced soil water content.

Mean nighttime CO_2 NEE (i.e. measured RE) was 6.9 ± 10.5 μmol m^{-2} s^{-1} and 6.5 ± 10.5 μmol m^{-2} s^{-1} in 2018 and 2019, respectively (Fig. S8). The mean nighttime RE was higher during the dry season (7.6 ± 11.0 μmol m^{-2} s^{-1}, 8.2 ± 11.3 μmol m^{-2} s^{-1}) compared to the wet season (5.9 ± 9.8 μmol m^{-2} s^{-1}, 5.7 ± 9.8 μmol m^{-2} s^{-1}) in both 2018 and 2019, respectively. Carswell et al. (2002) found that mean nighttime RE increased from about 7.1 μmol m^{-2} s^{-1} in the wet season to 8.2 μmol m^{-2} s^{-1} in the dry season for the Belém, Pará, Brazil site. Hutyra et al. (2007) showed that the mean nighttime RE was typically 9.2 μmol m^{-2} s^{-1} during the wet season and decreased to 7.7 μmol m^{-2} s^{-1} during the dry season for the Tapajós site. Thus, our nighttime

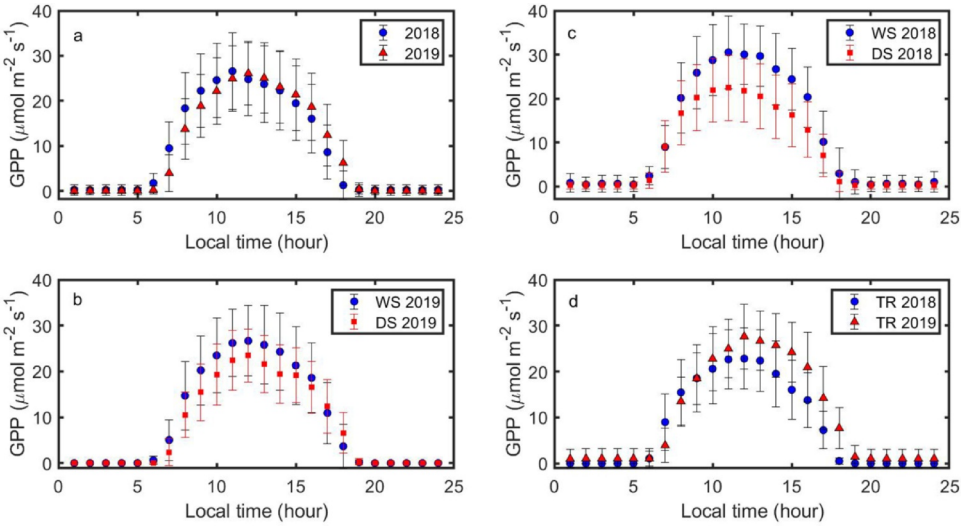

Fig. 10. Diel patterns of gross ecosystem photosynthesis (GEP). (a) all data; (b) wet season and dry season in 2018; (c) wet season and dry season in 2019; (d) transition season in 2018 and 2019.

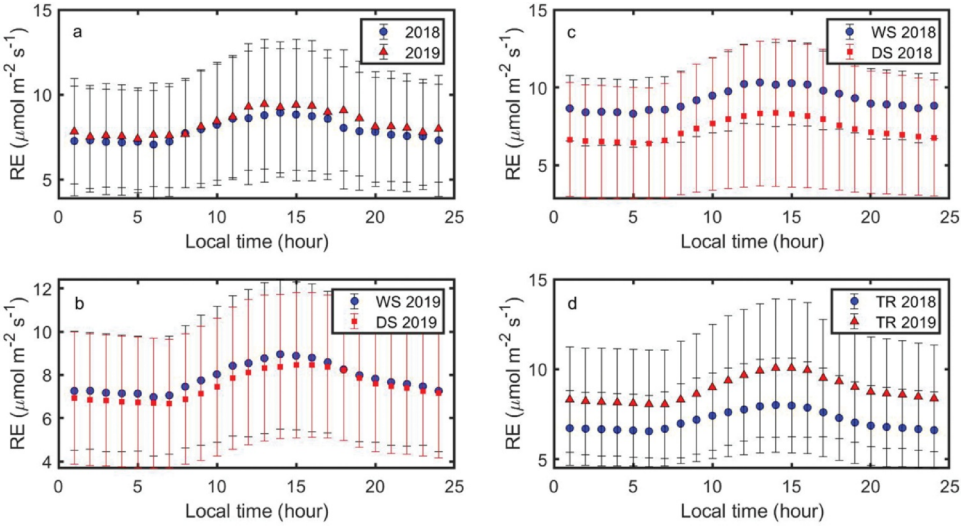

Fig. 11. Diel patterns of ecosystem respiration (RE). (a) all data; (b) wet season and dry season in 2018; (c) wet season and dry season in 2019; (d) transition season in 2018 and 2019.

values are comparable in terms of magnitude, and similar in seasonal pattern to the *terra firme* ecosystem. Nighttime RE did not show any significant relation with respect to soil temperature, air temperature or soil water content, but were proportional to GPP (Fig. S7). A similar conclusion was reported by Carswell et al. (2002) and Hutyra et al. (2007). This supports that the reduced net uptake of CO_2 during the dry season, or high temperature periods, was largely driven by a reduction in photosynthetic activity and a modest increase in RE.

3.3. Net ecosystem CH_4 exchange

The 2019 half-hourly CH_4 NEE values followed a skewed Laplace distribution, yielding a mean flux of 59.3 ± 89.3 nmol m^{-2} s^{-1}. We did not observe a pronounced diel pattern in CH_4 NEE, however, emissions during the wet season were consistently higher (mean = 59.5 ± 89.0 nmol m^{-2} s^{-1}) than during the dry season (mean = 46.9 ± 63.6 nmol m^{-2} s^{-1}) with a slight increase during midday for the wet period (Figs. 12 and S9,S10). Recent work by Deshmukh et al. (2020) observed a significant diel cycle in CH_4 emissions for a natural forested tropical peatland in Sumatra, Indonesia that was correlated with photosynthetic flux and canopy conductance. Tang et al. (2018) also reported a significant diel pattern in CH_4 emissions for a two-month study conducted in a tropical peat forest in Sarawak, Malaysian Borneo, highlighting the potential importance of plant-mediated transport of CH_4.

Higher variability of NEE CH_4 at night was likely associated with lower friction velocities and may indicate short-term variability in the total flux caused by changes in CH_4 storage or the influence of ebullition events during these more stable atmospheric conditions (i.e. weaker boundary-layer mixing). Weak positive relationships were observed between CH_4 NEE and soil temperature, air temperature, and water table position at the weekly timescale (Fig. 13), but were not statistically significant. This is likely related to the very small variations in soil temperature and water table position. Further, we found a weak positive relation (slope = 5.6 nmol m^{-2} s^{-1} kPa^{-1}) between CH_4 NEE and atmospheric pressure, but it was not statistically significant. Based on an analysis of the statistical distributions for high (>25 °C) vs low (<25 °C) temperatures, we found CH_4 fluxes to be very similar, 42.0 ± 66.7 nmol m^{-2} s^{-1} vs 42.3 ± 86.9 nmol m^{-2} s^{-1}, respectively (Figs. S11 and S12). However, there was some evidence of increasing CH_4 emissions with increasing *LE* (Fig. S13) and increasing CO_2 NEE magnitude (i.e increasing photosynthetic activity, Fig. 13), suggesting that plant-mediated transport might be important. For example, van Lent et al. (2019) showed a positive correlation between CH_4 fluxes and the *M. flexuosa* pneumatophore density. Indeed, Pangala et al.

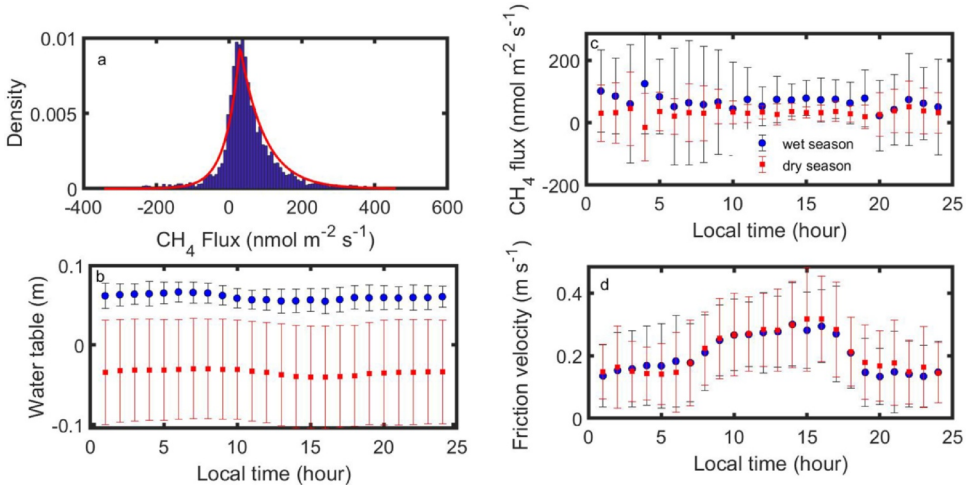

Fig. 12. Net ecosystem methane exchange. (a) half-hourly flux distribution in 2019; (b) diel patterns of friction velocity for the dry and wet seasons in 2019; (c) diel patterns of net ecosystem methane flux during the wet and dry seasons of 2019; (d) diel patterns of soil water content in 2019.

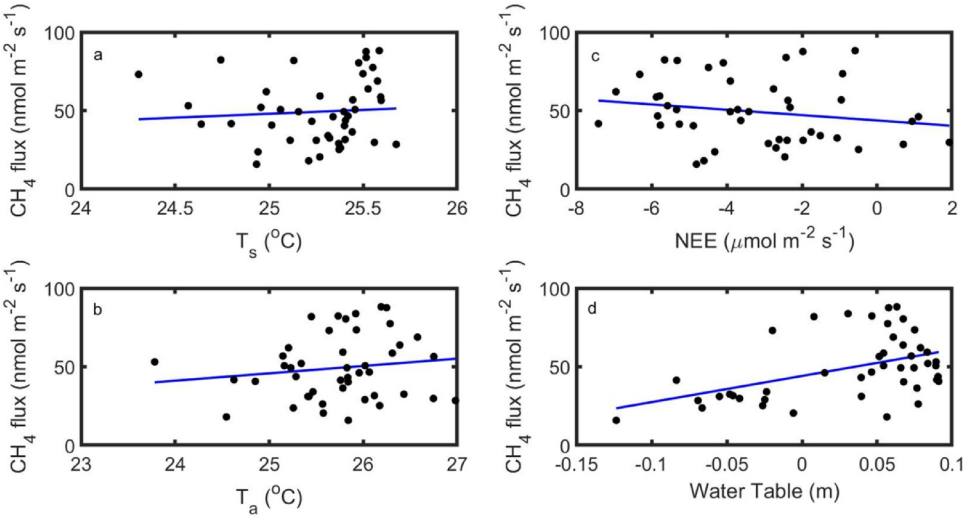

Fig. 13. Relationships between net ecosystem methane exchange averaged over 7-day periods for environmental drivers including: (a) soil temperature; (b) air temperature; (c) net ecosystem CO_2 exchange, and (d) water table position.

(2017) have shown that CH_4 emissions from central Amazonian tree stems were up to 200-fold greater than emissions from tropical peat swamp soils and the dominant diffusive flux component observed in the Amazonia. Tree bole CH_4 flux measurements have helped reconcile the large disparity observed between top-down and bottom-up CH_4 budget estimates for the Amazon Basin (Pangala et al., 2017).

Methane emissions have also been reported for a tropical peat swamp forest located in Sarawak, Malaysia based on the EC approach (Wong et al., 2018). They found that mean CH_4 emissions were 24.0 nmol m^{-2} s^{-1}, substantially lower compared to the Quistococha palm swamp forest. Their research showed little dependence of CH_4 emissions on water table position, soil water content, or soil temperature, presumably because of the low variability of these potential environmental drivers. Our EC CH_4 fluxes are higher than soil chamber fluxes (5.2 to 43.3 nmol m^{-2} s^{-1}) measured within the Quistococha Regional Park during the dry season of December 2011 and December 2012 (Finn et al., 2020) and are in relatively good agreement with *in situ* observations (mean annual flux densities ranging from 38.3 to 84.3 nmol m^{-2} s^{-1}) in the same park over the period April 2015 to March 2018 (Hergoualc'h et al., 2020). Further, laboratory incubations using soil samples extracted from within the Quistococha Regional Park, indicate a CH_4 emission potential on the order of 80 nmol m^{-2} s^{-1} (van Lent et al., 2019), which also supports our observations.

3.4. Carbon budget and net radiative forcing

Cumulative CO_2 NEE in 2018 and 2019 indicated an overall carbon sink of about −465 (−279 to −651) g C m^{-2} y^{-1} and −462 (−277 to −647) g C m^{-2} y^{-1}, respectively (Fig. 14). The uncertainty estimates (40% relative uncertainty) in parentheses were derived from the Monte Carlo and gap filling analyses. Overall, we cannot conclude that the cumulative seasonal pattern of CO_2 NEE, or its annual total, differed significantly between years. However, we note an important divergence between each year over the period DOY 250 (September 7) to DOY 325 (November 21) that relates to a decline in water table position in 2019 relative to 2018 (Fig. S4). Here, midday RE was enhanced by up to 4 μmol m^{-2} s^{-1} relative to the same period in 2018. These results further highlight the sensitivity of this palm swamp forest carbon balance to hydrometeorological conditions.

The cumulative CO_2 NEE values above include the so-called CO_2 open-path senor self-heating correction of Burba et al. (2008). When these corrections are not applied, the annual CO_2 NEE is estimated at −552 g C m^{-2} y^{-1} and −546 g C m^{-2} y^{-1} for 2018 and 2019,

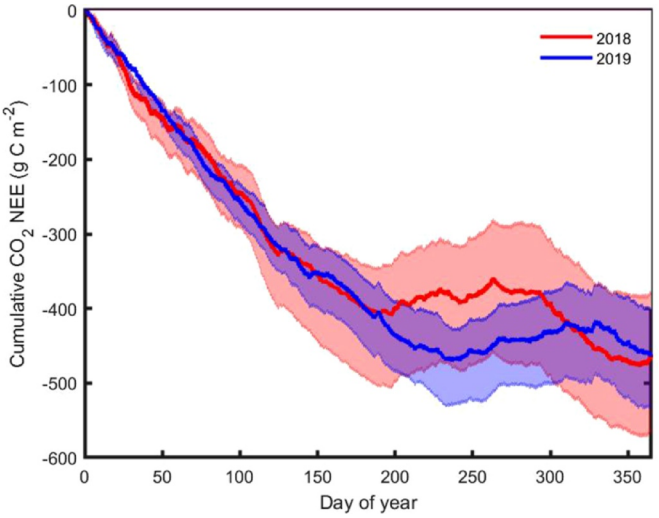

Fig. 14. Cumulative net ecosystem CO_2 exchange (NEE) in 2018 and 2019. Note that the uncertainty estimates were derived from a Monte Carlo approach that assesses the impact of the gap-filling approach on the cumulative NEE.

respectively. We note here that the sensor self-heating correction factors are highly uncertain for any given site due to site-specific variability in IRGA heat fluxes, and ambient temperature-specific IRGA measurement bias that both are unaccounted for in the correction framework (Deventer et al., 2020). It is, however, noteworthy that despite these large uncertainties, the differences in annual budget estimates calculated with and without applying the correction differ by ~85 g m^{-2} y^{-1} (~18 %), fall within the respective uncertainty bounds, and thus do not alter the conclusion that this palm swamp peatland is a large CO_2 sink.

The annual CH_4 NEE budget for 2019 was estimated to be a source of 22 (20 to 24) g CH_4-C m^{-2} y^{-1}, according to the monthly Laplace distribution analyses. Here, the uncertainty in parentheses was propagated from the range of the mean monthly values. The annual CH_4 NEE budget, based on the ANN approach was 17 (12 to 23) g CH_4-C m^{-2} y^{-1}. However, since the ANN budget approach was characterized by low predictive power (i.e. $R^2 < 0.1$) we make use of the Laplace distribution analyses. Monthly CH_4 emissions ranged from 1.0 to 2.7 g CH_4-C m^{-2} $month^{-1}$ (Fig. S14). Maximum monthly CH_4 emissions were generally correlated with monthly precipitation. The CH_4 NEE

Table 2
Summary of net ecosystem CH_4 exchange and soil CH_4 emissions of select peatland and wetland sites.

Site	Years	Ecosystem	Climate	Flux (g C m^{-2} y^{-1})	Reference
Iquitos, Peru, QFR 73° 19′ 08.1" W; 3° 50′ 03.9" S	2019	palm swamp peat forest	3000 mm; 26 °C	22[a]	this study
Iquitos, Peru, Quistococha Regional Reserve	2015-2018	intact palm swamp peat forest	3087 mm; 27 °C	14.5 to 31.9[b]	Hergoualc'h et al. (2020)
Maludam National Park, Sarawak, Malaysia 111° 8′ E 1° 27′ N	2014-2015	peat swamp forest	2540 mm 27.1 °C	9.2[a]	Wong et al. (2018)
Maludam National Park, Sarawak, Malaysia 111° 8′ E 1° 27′ N	2013	peat swamp forest	not reported for time period	8.8[a]	Tang et al. (2018)
Meta-analysis of sites from Southeast Asia	1990s-2010	intact peat swamp forest	26.3 °C	28.6[b,c]	Hergoualc'h and Verchot (2014)
Winous Point Marsh Conservancy, Lake Erie, Ohio, USA 82° 59′ 45.02" W; 41° 27′ 51.28" N	2011-2013	fresh water marsh	840 mm; 9.2 °C	42.3 to 57.0[a]	Chu et al. (2014)
Sacromento-San Joaquin Delta, CA, USA, 121.7650° W; 38.0498° N	2012-2013	restored young wetland	390 mm; 15 °C	53[a]	Knox et al. (2015)
Marcell Experimental Forest, Minnesota, USA -93.489° W 45.505° N	2015-2017	sub-boreal fen	770 mm 3 °C	10.7 to 15.1[a]	Deventer et al. (2019) Olson et al. (2013)
North Slope, Barrow, Alaska, USA 156° 36′ 33.04" W; 71° 19′ 21.10" N	2013-2014	wet sedge tundra	Not reported for time period	4.5[a]	Goodrich et al. (2016)
Lena River Delta, Siberia, Russia 126° 30′ E; 72° 22′ N	2003-2004	arctic tundra	319 mm; -14.7	2.4[a]	Wille et al. (2008)

*note that a positive NEE value indicates a CH_4 source; Climate statistics represent mean annual values.
[a] annual estimate of CH_4 NEE derived from eddy covariance data;
[b] annual estimate of soil CH_4 emissions derived from chamber data;
[c] annual mean derived from all available site data.

budget of the Quistococha palm swamp forest is in excellent agreement with chamber based estimates (14.5 to 31.9 g CH_4-C m^{-2} y^{-1}) within the park over the period April 2015 to March 2018 (Hergoualc'h et al., 2020). Methane emissions from the Quistococha site are larger than our mean budget estimate for a sub-boreal peatland (10.7 to 15.1 g CH_4-C m^{-2} y^{-1}) in Minnesota, USA (Deventer et al., 2019; Olson et al., 2013) and northern peatlands (Table 2) and substantially larger than that extrapolated from two months of wet season measurements (8.8 g CH_4-C m^{-2} y^{-1}) over a tropical peat forest in Sarawak, Malaysian Borneo (Tang et al., 2018). Further, our annual budget estimate is in excellent agreement with chamber-based estimates (28.6 ± 9.7 g CH_4-C m^{-2} y^{-1}) from intact peat swamp forests in Southeast Asia (Hergoualc'h and Verchot, 2014). A recent synthesis of global eddy covariance CH_4 flux measurements revealed that tropical wetlands were extremely underrepresented in the global database (Knox et al., 2019). They reported only three sites (freshwater marsh site, USA; swamp Maludam, Malaysia; and brackish marsh, USA) with an estimated mean annual emission of 43.2 ± 11.2 g CH_4-C m^{-2} y^{-1}.

The CO_2 sink strength of the Quistococha site was substantially higher than that of a tropical peat swamp forest in Sarawak, Malaysia, (mean of -136 ± 51 g C m^{-2} y^{-1}) over the period 2011 to 2014 (Kiew et al., 2018) and a peat swamp forest in Indonesia (mean of +174 ± 203 g C m^{-2} y^{-1}) over the period 2004 to 2008 (Hirano et al., 2012). Our review of tropical forest CO_2 budgets (Table 3) and comparison with the mean CO_2 NEE derived by Luyssaert et al. (2007) (see their Table 3, mean NEE = −403 ± 102 g C m^{-2} y^{-1}) indicates that the Quistococha site is a relatively large CO_2 sink, but within the range of reported values for other tropical forests. Previous studies have argued that the spatial and temporal patterns of the annual CO_2 budget in Amazonian forests can be large, ranging from sink to source depending on climate and disturbance factors (Saleska et al., 2003). Further, a recent synthesis examining the impacts of El Niño/La Niña on the carbon balance of tropical ecosystems provides strong evidence that the drier conditions associated with El Niño are likely to reduce their carbon sink strength through a reduction in photosynthetic fluxes (Gloor et al., 2018; Koren et al., 2018; Malhi et al., 2018). In the western Amazon, El Niño/La Niña events may be less important than the influence of warm tropical NTA-SST anomalies on climate (Chen et al., 2015; Lilleskov et al., 2019), which have been shown to increase drought and fire frequency in the region. Model simulations by Wang et al. (2018) suggest that the peatlands of the Pastaza-Marañon Foreland Basin are susceptible to changing from a carbon sink to a carbon source if conditions continue to get warmer and drier within the region. Our observations and analyses for an underrepresented Amazonian palm swamp peatland in the Pastaza-Marañon Foreland Basin strongly support these findings.

The current rate of carbon accumulation, as measured from EC, cannot be compared directly to the long-term apparent rate of carbon accumulation (LARCA) as derived from peat core data (Ratcliffe et al., 2018; Young et al., 2019) because carbon accumulated in the current year has undergone less decomposition than older peats, which continue to lose carbon for thousands of years (Clymo et al., 1998). In fact, most of the recently accumulated carbon will not become part of the long-term peat. This is why the contemporary carbon balance of the Quistococha palm swamp forest is large (average sink = 464 g C m^{-2} y^{-1}) relative to the long-term apparent peat carbon accumulation rate (LARCA = 74 g C m^{-2} y^{-1}). Additional reasons for this disparity could also be related to: (1) a short record of EC measurements that do not capture the potential range of inter-annual variability of NEE at this site; (2) the dynamic history of paleo-vegetation; and (3) potential carbon losses in the form of disturbance and/or lateral DOC/DIC exports. Paleoecological evidence shows that the vegetation has changed dramatically at this site over the past 200 years (Lähteenoja et al., 2009b) suggesting a potential for periods of disturbance and net carbon losses (Saleska et al., 2003). The site is located in close proximity to the Amazon river network so that channel meandering and avulsion have the potential to cause disturbances by removing or burying peat carbon (Salo et al., 1986). Drainage likely represents a significant carbon export from this watershed. Hastie et al. (2019) have shown that there is large inter-annual variability in the net carbon export from Amazonian river flood plains, which represents a significant fraction of carbon fixed by these forest ecosystems. Indeed, our energy balance measurements indicated that annual evaporation accounted for only 36% of the annual precipitation, which implies that drainage and runoff are significant. Measurements of DOC/DIC transport, however, have not yet been estimated for these palm swamp peatlands and this represents a

Table 3
Summary of net ecosystem CO_2 exchange of select tropical forest sites.

Site	Years	Ecosystem	Climate	NEE (g C m^{-2} y^{-1})	Reference
Iquitos, Peru, QFR 73° 19′ 08.1" W; 3° 50′ 03.9" S	2018 to 2019	palm swamp peat forest	3000 mm; 26 °C	range of -462 to -465	this study
Sarawak, Malaysia 111° 24′ E 1° 23′ N	2011 to 2014	peat swamp forest	26.5 °C	range of -207 to -98	Kiew et al. (2018)
Palangkaraya, Indonesia	July 2004 to July 2008	peat swamp secondary forest	2452 mm 26 °C	range of -27 to +443	Hirano et al. (2012)
Pasoh Forest Reserve, Peninsular Malaysia 102° 18′ E; 2° 58′ N	2003 to 2005	lowland tropical evergreen forest	1804 mm	-147 to -79	Kosugi et al. (2008)
French Guiana, South America 52° 54′ W; 5° 16′ N	2004 to 2005	pristine tropical wet forest	3041 mm; 26.5 °C	-157 to -142	Bonal et al. (2008)
Tapajós National Forest, Pará, Brazil 54° 58′ W 2° 51′ S	2002 to 2005	evergreen old growth tropical rain forest	2200 mm 26 °C	range of -221 to +2677	Hutyra et al. (2007)
Tapajós National Forest, Pará, Brazil 54° 58′ W 2° 51′ S 54° 56′ W 3° 54′ S Sites KM 67 and KM 83	July 2000 to August 2003	Evergreen old growth tropical rain forest	25 °C 1920 mm	range of +0 to +2300	Saleska et al. (2003)
Cuieiras Forest Reserve, near Manaus, Brazil 60° 06′ 55" W; 2° 35′ 22" S	Sept 1, 1995 to Aug 31, 1996	lowland terra firme tropical rain forest	2200 mm	-590	Malhi et al. (1998)
Reserva, Jaru, Rondonia, Brazil, 61° 56′ W; 10° 84′ S	Sept 1992; April to June 1993	old growth tropical rain forest	1997 mm 25 °C	-102[a]	Grace et al. (1995)
Reserva Florestal Ducke, near Manaus, Brazil 59° 57′ W; 2° 57′ S	April 22 to May 8, 1987	old tropical rain forest	1415 mm 27 °C	-220[b]	Fan et al. (1990)

*note that a negative NEE value indicates a CO_2 sink;
[a] annual estimate derived from a model parameterized with site data;
[b] annual estimate based on mean flux value;

potentially large uncertainty in our carbon accounting.

A global warming potential (GWP) analysis, based on the annual budgets of contemporary CO_2 and CH_4 flux measurements, does not necessarily reflect the long-term carbon dynamics of a peatland or the temporal dynamics and equilibrium response times of radiative forcing associated with changes in atmospheric burdens of CO_2 and CH_4 (Frolking et al., 2006; Neubauer, 2014). Here, we estimate the GWP to help assess the relative importance of contemporary CH_4 emissions versus CO_2 uptake on the climate system. The GWP, on a 100-year time horizon, for CH_4 is estimated at 28 with no carbon cycle feedbacks and 34 when including these feedbacks (Myhre et al., 2013). Therefore, based on the above annual budget estimates, the CO_2 equivalence of the CH_4 emissions is estimated to be 821 to 997 g CO_{2eq} m^{-2} y^{-1}, indicating that this Amazonian palm swamp peatland has a net negative radiative forcing effect in terms of its CO_2 budget (i.e. after converting from CO_2-C to CO_2, 1705 g CO_2 m^{-2} y^{-1} and 1694 g CO_2 m^{-2} y^{-1}) and CH_4 budgets. However, this does not include the potential impacts of DIC/DOC transport and cycling offsite. Further, the sensitivity of NEE CO_2 to warmer and drier conditions implies that the carbon sink of these palm swamp peatlands could be reduced substantially by increasing tropical temperatures (Gloor et al., 2018) or through the increased intensity or frequency of drought events. Such feedbacks require longer-term observations to help understand the potential role of acclimation in these systems.

4. Conclusions

Our research has provided the first observations and analyses of the energy, CO_2, and CH_4 balance of an Amazonian palm swamp forested peatland. The results suggest that these peatlands may be an important CO_2 sink and a CH_4 source. While light-response analyses and flux partitioning support that photosynthetic activity in these systems is inhibited by high photosynthetic photon flux density, air temperatures, and vapor pressure deficits, latent heat flux appeared to be insensitive to these climate drivers. There is also evidence for increased ecosystem respiration under drier conditions and lower water table positions. Methane emissions were enhanced during the wet season, but did not show a significant diel pattern or temperature dependence. Overall, the CH_4 NEE budget was similar to that reported for other tropical peatlands and generally larger than sub-boreal and northern peatlands. Considering the global warming potential of CH_4 on a 100-year time horizon, we estimate that these ecosystems have a net radiative cooling effect in terms of their carbon budget. Further research is required to reduce the uncertainties in the annual carbon budget, carbon losses associated with runoff and drainage, and the processes controlling CH_4 production, consumption, and transport between the ecosystem and atmosphere. This is a very challenging environment for conducting long-term eddy covariance observations, but such measurements are critical to understanding the longer-term feedbacks associated with changes in hydrometeorological forcings.

Declaration of Competing Interest

The authors declare that they have no known competing financial interests or personal relationships that could have appeared to influence the work reported in this paper.

Acknowledgments

This material is based upon work supported by the U.S. Department of Energy, Office of Science, Office of Biological and Environmental Research, Terrestrial Ecosystem Science Program, under Award Number DE-SC0020167. JDW acknowledges support provided by the U.S. Department of Energy, Office of Science, Office of Biological and Environmental Research Program, Oak Ridge National Laboratory's Terrestrial Ecosystem Science-Science Focus Area; ORNL is managed by UT- Battelle, LLC, for the U.S. Department of Energy under contract DE-AC05-00OR22725. This material is also based on work supported by

the U.S. interagency SilvaCarbon program and the Sustainable Wetlands Adaptation and Mitigation Program (SWAMP) program. SilvaCarbon is funded by the U.S. Agency for International Development (USAID) and U.S. Department of State, and is implemented by the U.S. Forest Service (USFS) and U.S. Geological Survey. SWAMP is funded by USAID and implemented by USFS and the Center for International Forestry Research. HCQ's contribution was supported by the U.S. National Science Foundation under Grant No 1355066. The data used to support this work have been submitted to the AmeriFlux program and available for download at: https://ameriflux.lbl.gov/sites/siteinfo/PE-QFR.

Supplementary materials

Supplementary material associated with this article can be found, in the online version, at doi:10.1016/j.agrformet.2020.108167.

References

Baldocchi, D.D., Hicks, B.B., Meyers, T.P., 1988. Measuring biosphere-atmosphere exchanges of biologically related gases with micrometeorological methods. Ecology. https://doi.org/10.2307/1941631.

Bhomia, R.K., van Lent, J., Rios, J.M.G., Hergoualc'h, K., Coronado, E.N.H., Murdiyarso, D., 2019. Impacts of Mauritia flexuosa degradation on the carbon stocks of freshwater peatlands in the Pastaza-Marañón river basin of the Peruvian Amazon. Mitig. Adapt. Strateg. Glob. Chang. https://doi.org/10.1007/s11027-018-9809-9.

Blanken, P.D., Rouse, W.R., 1996. Evidence of water conservation mechanisms in several subarctic wetland species. J. Appl. Ecol. https://doi.org/10.2307/2404954.

Bonal, D., Bosc, A., Ponton, S., Goret, J.Y., Burban, B.T., Gross, P., Bonnefond, J.M., Elbers, J., Longdoz, B., Epron, D., Guehl, J.M., Granier, A., 2008. Impact of severe dry season on net ecosystem exchange in the Neotropical rainforest of French Guiana. Glob. Chang. Biol. https://doi.org/10.1111/j.1365-2486.2008.01610.x.

Buckley, T.N., 2019. How do stomata respond to water status? New Phytol. https://doi.org/10.1111/nph.15899.

Buckley, T.N., 2017. Modeling stomatal conductance. Plant Physiol. https://doi.org/10.1104/pp.16.01772.

Burba, G.G., McDermitt, D.K., Grelle, A., Anderson, D.J., Xu, L., 2008. Addressing the influence of instrument surface heat exchange on the measurements of CO2 flux from open-path gas analyzers. Glob. Chang. Biol. 14, 1854–1876. https://doi.org/10.1111/j.1365-2486.2008.01606.x.

Carswell, F.E., Costa, A.L., Palheta, M., Malhi, Y., Meir, P., Costa, J.D.P.R., Ruivo, M.D.L., Leal, L.D.S.M., Costa, J.M.N., Clement, R.J., Grace, J., 2002. Seasonality in CO2 and H2O flux at an eastern Amazonian rain forest. J. Geophys. Res. D Atmos. https://doi.org/10.1029/2000JD000284.

Chen, Y., Randerson, J.T., Morton, D.C., 2015. Tropical North Atlantic ocean-atmosphere interactions synchronize forest carbon losses from hurricanes and Amazon fires. Geophys. Res. Lett. https://doi.org/10.1002/2015GL064505.

Chu, H., Chen, J., Gottgens, J.F., Ouyang, Z., John, R., Czajkowski, K., Becker, R., 2014. Net ecosystem methane and carbon dioxide exchanges in a Lake Erie coastal marsh and a nearby cropland. J. Geophys. Res. Biogeosciences. https://doi.org/10.1002/2013JG002520.

Clymo, R.S., Turunen, J., Tolonen, K., 1998. Carbon Accumulation in Peatland. Oikos. https://doi.org/10.2307/3547057.

Da Rocha, H.R., Manzi, A.O., Cabral, O.M., Miller, S.D., Goulden, M.L., Saleska, S.R., Coupe, N.R., Wofsy, S.C., Borma, L.S., Artaxo, R., Vourlitis, G., Nogueira, J.S., Cardoso, F.L., Nobre, A.D., Kruijt, B., Freitas, H.C., Von Randow, C., Aguiar, R.G., Maia, J.F., 2009. Patterns of water and heat flux across a biome gradient from tropical forest to savanna in Brazil. J. Geophys. Res. Biogeosciences. https://doi.org/10.1029/2007JG000640.

Dargie, G.C., Lewis, S.L., Lawson, I.T., Mitchard, E.T.A., Page, S.E., Bocko, Y.E., Ifo, S.A., 2017. Age, extent and carbon storage of the central Congo Basin peatland complex. Nature. https://doi.org/10.1038/nature21048.

Deshmukh, C.S., Julius, D., Evans, C.D., Nardi, Susanto, A.P., Page, S.E., Gauci, V., Laurén, A., Sabiham, S., Agus, F., Asyhari, A., Kurnianto, S., Suardiwerianto, Y., Desai, A.R., 2020. Impact of forest plantation on methane emissions from tropical peatland. Glob. Chang. Biol. https://doi.org/10.1111/gcb.15019.

Deventer, M.J., Bogoev, I., Roman, T., Kolka, R.K., Erickson, M., Lee, X., Baker, J.M., Millet, D.B., Griffis, T.J., 2020. Biases in open-path carbon dioxide flux measurements: Roles of instrument surface heat exchange and analyzer temperature sensitivity. Agric. For. Meteorol in review.

Deventer, M.J., Griffis, T.J., Roman, D.T., Kolka, R.K., Wood, J.D., Erickson, M., Baker, J.M., Millet, D.B., 2019. Error characterization of methane fluxes and budgets derived from a long-term comparison of open- and closed-path eddy covariance systems. Agric. For. Meteorol. 278, 107638. https://doi.org/10.1016/j.agrformet.2019.107638.

Draper, F.C., Roucoux, K.H., Lawson, I.T., Mitchard, E.T.A., Honorio Coronado, E.N., Lähteenoja, O., Montenegro, L.T., Sandoval, E.V., Zaráte, R., Baker, T.R., 2014. The distribution and amount of carbon in the largest peatland complex in Amazonia. Environ. Res. Lett. https://doi.org/10.1088/1748-9326/9/12/124017.

Falge, E., Baldocchi, D., Olson, R., Anthoni, P., Aubinet, M., Bernhofer, C., Burba, G., Ceulemans, R., Clement, R., Dolman, H., Granier, A., Gross, P., Grünwald, T., Hollinger, D., Jensen, N.O., Katul, G., Keronen, P., Kowalski, A., Lai, C.T., Law, B.E., Meyers, T., Moncrieff, J., Moors, E., Munger, J.W., Pilegaard, K., Rannik, Ü., Rebmann, C., Suyker, A., Tenhunen, J., Tu, K., Verma, S., Vesala, T., Wilson, K., Wofsy, S., 2001. Gap filling strategies for defensible annual sums of net ecosystem exchange. Agric. For. Meteorol. https://doi.org/10.1016/S0168-1923(00)00225-2.

Fan, Song-Miao, Wofsy, S.C., Bakwin, P.S., Jacob, D.J., Fitzjarrald, D.R., 1990. Atmosphere-biosphere exchange of CO2 and O3 in the central Amazon forest. J. Geophys. Res. https://doi.org/10.1029/jd095id10p16851.

Finn, D., Robert, Ziv-el, M., Haren, Van, J., Park, J.G., 2020. Methanogens and methanotrophs show nutrient-dependent community assemblage patterns across tropical peatlands of the pastaza-Marañón Basin. Peruvian Amazonia 11, 1–15. https://doi.org/10.3389/fmicb.2020.00746.

Fisher, J.B., Malhi, Y., Bonal, D., Da Rocha, H.R., De Araújo, A.C., Gamo, M., Goulden, M.L., Rano, T.H., Huete, A.R., Kondo, H., Kumagai, T., Loescher, H.W., Miller, S., Nobre, A.D., Nouvellon, Y., Oberbauer, S.F., Panuthai, S., Roupsard, O., Saleska, S., Tanaka, K., Tanaka, N., Tu, K.P., Von Randow, C., 2009. The land-atmosphere water flux in the tropics. Glob. Chang. Biol. https://doi.org/10.1111/j.1365-2486.2008.01813.x.

Fonseca, L.D.M., Dalagnol, R., Malhi, Y., Rifai, S.W., Costa, G.B., Silva, T.S.F., Da Rocha, H.R., Tavares, I.B., Borma, L.S., 2019. Phenology and seasonal ecosystem productivity in an Amazonian floodplain forest. Remote Sens. https://doi.org/10.3390/rs11131530.

Frankenberg, C., Meirink, J.F., Van Weele, M., Platt, U., Wagner, T., 2005. Assessing methane emissions from global space-borne observations. Science. https://doi.org/10.1126/science.1106644.

Fratini, G., Ibrom, A., Arriga, N., Burba, G., Papale, D., 2012. Relative humidity effects on water vapour fluxes measured with closed-path eddy-covariance systems with short sampling lines. Agric. For. Meteorol. 165, 53–63. https://doi.org/10.1016/j.agrformet.2012.05.018.

Frolking, S., Roulet, N., Fuglestvedt, J., 2006. How northern peatlands influence the Earth's radiative budget: Sustained methane emission versus sustained carbon sequestration. J. Geophys. Res. Biogeosciences. https://doi.org/10.1029/2005JG000091.

Gloor, E., Wilson, C., Chipperfield, M.P., Chevallier, F., Buermann, W., Boesch, H., Parker, R., Somkuti, P., Gatti, L.V., Correia, C., Domingues, L.G., Peters, W., Miller, J., Deeter, M.N., Sullivan, M.J.P., 2018. Tropical land carbon cycle responses to 2015/16 El Niño as recorded by atmospheric greenhouse gas and remote sensing data. Philos. Trans. R. Soc. B Biol. Sci. 373. https://doi.org/10.1098/rstb.2017.0302.

Goodrich, J.P., Oechel, W.C., Gioli, B., Moreaux, V., Murphy, P.C., Burba, G., Zona, D., 2016. Impact of different eddy covariance sensors, site set-up, and maintenance on the annual balance of CO2 and CH4 in the harsh Arctic environment. Agric. For. Meteorol. https://doi.org/10.1016/j.agrformet.2016.07.008.

Grace, J, Lloyd, J., McIntyre, J., Miranda, A.C., Meir, P., Miranda, H.S., Nobre, C., Moncrieff, J., Massheder, J., Malhi, Y., Wright, I., Gash, J., 1995. Carbon-dioxide uptake by an undisturbed tropical rain-forest in Southwest Amazonia, 1992 to 1993 15. Science) 270, 778–780.

Griffis, T.J., Black, T.A., Morgenstern, K., Barr, A.G., Nesic, Z., Drewitt, G.B., Gaumont-Guay, D., McCaughey, J.H., 2003. Ecophysiological controls on the carbon balances of three southern boreal forests. Agric. For. Meteorol. 117, 53–71.

Gumbricht, T., Roman-Cuesta, R.M., Verchot, L., Herold, M., Wittmann, F., Householder, E., Herold, N., Murdiyarso, D., 2017. An expert system model for mapping tropical wetlands and peatlands reveals South America as the largest contributor. Glob. Chang. Biol. https://doi.org/10.1111/gcb.13689.

Hastie, A., Lauerwald, R., Ciais, P., Regnier, P., 2019. Aquatic carbon fluxes dampen the overall variation of net ecosystem productivity in the Amazon basin: An analysis of the interannual variability in the boundless carbon cycle. Glob. Chang. Biol. https://doi.org/10.1111/gcb.14620.

Hergoualc'h, K., Dezzeo, N., Verchot, L.V., Martius, C., van Lent, J., del Aguila Pasquel, J., Lopez, M., 2020. Spatial and temporal variability of soil N2O and CH4 fluxes along a degradation gradient in a palm swamp peat forest in the Peruvian Amazonle. Glob. Chang. Biol In press.

Hergoualc'h, K., Gutiérrez-Vélez, V.H., Menton, M., Verchot, L.V., 2017. Characterizing degradation of palm swamp peatlands from space and on the ground: An exploratory study in the Peruvian Amazon. For. Ecol. Manage. https://doi.org/10.1016/j.foreco.2017.03.016.

Hergoualc'h, K., Verchot, L.V., 2014. Greenhouse gas emission factors for land use and land-use change in Southeast Asian peatlands. Mitig. Adapt. Strateg. Glob. Chang. https://doi.org/10.1007/s11027-013-9511-x.

Hirano, T., Segah, H., Kusin, K., Limin, S., Takahashi, H., Osaki, M., 2012. Effects of disturbances on the carbon balance of tropical peat swamp forests. Glob. Chang. Biol. https://doi.org/10.1111/j.1365-2486.2012.02793.x.

Horst, T.W., Lenschow, D.H., 2009. Attenuation of scalar fluxes measured with spatially-displaced sensors. Boundary-Layer Meteorol. https://doi.org/10.1007/s10546-008-9348-0.

Huete, A.R., Didan, K., Shimabukuro, Y.E., Ratana, P., Saleska, S.R., Hutyra, L.R., Yang, W., Nemani, R.R., Myneni, R., 2006. Amazon rainforests green-up with sunlight in dry season. Geophys. Res. Lett. 33, 2–5. https://doi.org/10.1029/2005GL025583.

Hutyra, L.R., Munger, J.W., Saleska, S.R., Gottlieb, E., Daube, B.C., Dunn, A.L., Amaral, D.F., de Camargo, P.B., Wofsy, S.C., 2007. Seasonal controls on the exchange of carbon and water in an Amazonian rain forest. J. Geophys. Res. Biogeosciences. https://doi.org/10.1029/2006JG000365.

Kelly, T.J., Lawson, I.T., Roucoux, K.H., Baker, T.R., Jones, T.D., Sanderson, N.K., 2017. The vegetation history of an Amazonian domed peatland. Palaeogeogr. Palaeoclimatol. Palaeoecol. https://doi.org/10.1016/j.palaeo.2016.11.039.

Kiew, F., Hirata, R., Hirano, T., Wong, G.X., Aeries, E.B., Musin, K.K., Waili, J.W., Lo, K.S.,

Shimizu, M., Melling, L., 2018. CO2 balance of a secondary tropical peat swamp forest in Sarawak, Malaysia. Agric. For. Meteorol. https://doi.org/10.1016/j.agrformet.2017.10.022.
Kirschke, S., Bousquet, P., Ciais, P., Saunois, M., Canadell, J.G., Dlugokencky, E.J., Bergamaschi, P., Bergmann, D., Blake, D.R., Bruhwiler, L., Cameron-Smith, P., Castaldi, S., Chevallier, F., Feng, L., Fraser, A., Heimann, M., Hodson, E.L., Houweling, S., Josse, B., Fraser, P.J., Krummel, P.B., Lamarque, J.F., Langenfelds, R.L., Le Quéré, C., Naik, V., O'doherty, S., Palmer, P.I., Pison, I., Plummer, D., Poulter, B., Prinn, R.G., Rigby, M., Ringeval, B., Santini, M., Schmidt, M., Shindell, D.T., Simpson, I.J., Spahni, R., Steele, L.P., Strode, S.A., Sudo, K., Szopa, S., Van Der Werf, G.R., Voulgarakis, A., Van Weele, M., Weiss, R.F., Williams, J.E., Zeng, G., 2013. Three decades of global methane sources and sinks. Nat. Geosci. https://doi.org/10.1038/ngeo1955.
Kljun, N., Calanca, P., Rotach, M.W., Schmid, H.P., 2015. A simple two-dimensional parameterisation for Flux Footprint Prediction (FFP). Geosci. Model Dev. https://doi.org/10.5194/gmd-8-3695-2015.
Knox, S.H., Jackson, R.B., Poulter, B., McNicol, G., Fluet-Chouinard, E., Zhang, Z., Hugelius, G., Bousquet, P., Canadell, J.G., Saunois, M., Papale, D., Chu, H., Keenan, T.F., Baldocchi, D., Torn, M.S., Mammarella, I., Trotta, C., Aurela, M., Bohrer, G., Campbell, D.I., Cescatti, A., Chamberlain, S., Chen, J., Chen, W., Dengel, S., Desai, A.R., Euskirchen, E., Friborg, T., Gasbarra, D., Goded, I., Goeckede, M., Heimann, M., Helbig, M., Hirano, T., Hollinger, D.Y., Iwata, H., Kang, M., Klatt, J., Krauss, K.W., Kutzbach, L., Lohila, A., Mitra, B., Morin, T.H., Nilsson, M.B., Niu, S., Noormets, A., Oechel, W.C., Peichl, M., Peltola, O., Reba, M.L., Richardson, A.D., Runkle, B.R.K., Ryu, Y., Sachs, T., Schäfer, K.V.R., Schmid, H.P., Shurpali, N., Sonnentag, O., Tang, A.C.I., Ueyama, M., Vargas, R., Vesala, T., Ward, E.J., Windham-Myers, L., Wohlfahrt, G., Zona, D., 2019. FluXNET-CH4 synthesis activity objectives, observations, and future directions. Bull. Am. Meteorol. Soc. https://doi.org/10.1175/BAMS-D-18-0268.1.
Knox, S.H., Sturtevant, C., Matthes, J.H., Koteen, L., Verfaillie, J., Baldocchi, D., 2015. Agricultural peatland restoration: Effects of land-use change on greenhouse gas (CO2 and CH4) fluxes in the Sacramento-San Joaquin Delta. Glob. Chang. Biol. https://doi.org/10.1111/gcb.12745.
Koren, G., Van Schaik, E., Araújo, A.C., Boersma, K.F., Gärtner, A., Killaars, L., Kooreman, M.L., Kruijt, B., Van Der Laan-Luijkx, I.T., Von Randow, C., Smith, N.E., Peters, W., 2018. Widespread reduction in sun-induced fluorescence from the Amazon during the 2015/2016 El Niño. Philos. Trans. R. Soc. B Biol. Sci. 373. https://doi.org/10.1098/rstb.2017.0408.
Körner, C., 1995. Leaf diffusive conductances in the major vegetation types of the globe. Ecophysiol. Photosynth. https://doi.org/10.1007/978-3-642-79354-7_22.
Kosugi, Y., Takanashi, S., Ohkubo, S., Matsuo, N., Tani, M., Mitani, T., Tsutsumi, D., Nik, A.R., 2008. CO2 exchange of a tropical rainforest at Pasoh in Peninsular Malaysia. Agric. For. Meteorol. https://doi.org/10.1016/j.agrformet.2007.10.007.
Lähteenoja, O., Ruokolainen, K., Schulman, L., Alvarez, J., 2009a. Amazonian floodplains harbour minerotrophic and ombrotrophic peatlands. Catena. https://doi.org/10.1016/j.catena.2009.06.006.
Lähteenoja, O., Ruokolainen, K., Schulman, L., Oinonen, M., 2009b. Amazonian peatlands: An ignored C sink and potential source. Glob. Chang. Biol. https://doi.org/10.1111/j.1365-2486.2009.01920.x.
Landsberg, J.J., Gower, S.T., 1997. Ecosystem Process Models. Appl. Physiolog. Ecol.Forest Manag. https://doi.org/10.1016/b978-012435955-0/50009-1.
Lasslop, G., Reichstein, M., Papale, D., Richardson, A., Arneth, A., Barr, A., Stoy, P., Wohlfahrt, G., 2010. Separation of net ecosystem exchange into assimilation and respiration using a light response curve approach: Critical issues and global evaluation. Glob. Chang. Biol. https://doi.org/10.1111/j.1365-2486.2009.02041.x.
Leifeld, J., Menichetti, L., 2018. The underappreciated potential of peatlands in global climate change mitigation strategies /704/47/4113 /704/106/47 article. Nat. Commun. https://doi.org/10.1038/s41467-018-03406-6.
Lilleskov, E., McCullough, K., Hergoualc'h, K., del Castillo Torres, D., Chimner, R., Murdiyarso, D., Kolka, R., Bourgeau-Chavez, L., Hribljan, J., del Aguila Pasquel, J., Wayson, C., 2019. Is Indonesian peatland loss a cautionary tale for Peru? A two-country comparison of the magnitude and causes of tropical peatland degradation. Mitig. Adapt. Strateg. Glob. Chang. https://doi.org/10.1007/s11027-018-9790-3.
Lloyd, J., Taylor, J.A., 1994. On the Temperature Dependence of Soil Respiration. Funct. Ecol. https://doi.org/10.2307/2389824.
Luyssaert, S., Inglima, I., Jung, M., Richardson, A.D., Reichstein, M., Papale, D., Piao, S.L., Schulze, E.D., Wingate, L., Matteucci, G., Aragao, L., Aubinet, M., Beer, C., Bernhofer, C., Black, K.G., Bonal, D., Bonnefond, J.M., Chambers, J., Ciais, P., Cook, B., Davis, K.J., Dolman, A.J., Gielen, B., Goulden, M., Grace, J., Granier, A., Grelle, A., Griffis, T., Grunwald, T., Guidolotti, G., Hanson, P.J., Harding, R., Hollinger, D.Y., Hutyra, L.R., Kolari, P., Kruijt, B., Kutsch, W., Lagergren, F., Laurila, T., 2007. CO2-balance of boreal, temperate and tropical forests derived from a global database. Glob. Chang. Biol. 13, 2509–2537. https://doi.org/10.1111/j.1365-2486.2007.01439.x.
Malhi, Y., Nobre, A.D., Grace, J., Kruijt, B., Pereira, M.G.P., Culf, A., Scott, S., 1998. Carbon dioxide transfer over a Central Amazonian rain forest. J. Geophys. Res. Atmos. https://doi.org/10.1029/98JD02647.
Malhi, Y., Pegoraro, E., Nobre, A.D., Pereira, M.G.P., Grace, J., Culf, A.D., Clement, R., 2002. Energy and water dynamics of a central Amazonian rain forest. J. Geophys. Res. D Atmos. https://doi.org/10.1029/2001JD000623.
Malhi, Y., Rowland, L., Aragão, L.E.O.C., Fisher, R.A., 2018. New insights into the variability of the tropical land carbon cycle from the El Niño of 2015/2016. Philos. Trans. R. Soc. B Biol. Sci. 373. https://doi.org/10.1098/rstb.2017.0298.
McDermitt, D., Burba, G., Xu, L., Anderson, T., Komissarov, A., Riensche, B., Schedlbauer, J., Starr, G., Zona, D., Oechel, W., Oberbauer, S., Hastings, S., 2011. A new low-power, open-path instrument for measuring methane flux by eddy covariance. Appl. Phys. B 102, 391–405. https://doi.org/10.1007/s00340-010-4307-0.
Moncrieff, J., Clement, R., Finnigan, J., Meyers, T., 2006. Averaging, Detrending, and Filtering of Eddy Covariance Time Series. Handbook of Micrometeorology. https://doi.org/10.1007/1-4020-2265-4_2.
Montzka, S.A., Krol, M., Dlugokencky, E., Hall, B., Jöckel, P., Lelieveld, J., 2011. Small interannual variability of global atmospheric hydroxyl. Science (80-.). https://doi.org/10.1126/science.1197640.
Morgenstern, K., Black, T.A., Humphreys, E.R., Griffis, T.J., Drewitt, G.B., Cai, T., Nesic, Z., Spittlehouse, D.L., Livingston, N.J., 2004. Sensitivity and uncertainty of the carbon balance of a Pacific Northwest Douglas-fir forest during an El Niño/La Niña cycle. Agric. For. Meteorol. 123. https://doi.org/10.1016/j.agrformet.2003.12.003.
Myhre, G., Shindell, D., Bréon, F.-M., Collins, W., Fuglestvedt, J., Huang, J., Koch, D., Lamarque, J.-F., Lee, D., Mendoza, B., Nakajima, T., Robock, A., Stephens, G., Takemura, T., Zhang, H., 2013. Anthropogenic and Natural Radiative Forcing. Clim. Chang. 2013 Phys. Sci. Basis. Contrib. Work. Gr. I to Fifth Assess. Rep. Intergov. Panel Clim. Chang. 659–740. https://doi.org/10.1017/CBO9781107415324.018.
Myneni, R., Knyazikhin, Y., Park, T., 2015. MCD15A2H MODIS/Terra + Aqua Leaf Area Index/FPAR 8-Day L4 Global 500m SIN Grid V006. NASA EOSDIS L. Process. DAAC. https://doi.org/10.5067/MODIS/MCD15A2H.006.
Myneni, R.B., Yang, W., Nemani, R.R., Huete, A.R., Dickinson, R.E., Knyazikhin, Y., Didan, K., Fu, R., Negrón Juárez, R.I., Saatchi, S.S., Hashimoto, H., Ichii, K., Shabanov, N.V., Tan, B., Ratana, P., Privette, J.L., Morisette, J.T., Vermote, E.F., Roy, D.P., Wolfe, R.E., Friedl, M.A., Running, S.W., Votava, P., El-Saleous, N., Devadiga, S., Su, Y., Salomonson, V.V., 2007. Large seasonal swings in leaf area of Amazon rainforests. Proc. Natl. Acad. Sci. U. S. A. https://doi.org/10.1073/pnas.0611338104.
Nemitz, E., Mammarella, I., Ibrom, A., Aurela, M., Burba, G.G., Dengel, S., Gielen, B., Grelle, A., Heinesch, B., Herbst, M., Hörtnagl, L., Klemedtsson, L., Lindroth, A., Lohila, A., McDermitt, D.K., Meier, P., Merbold, L., Nelson, D., Nicolini, G., Nilsson, M.B., Peltola, O., Rinne, J., Zahniser, M., 2018. Standardisation of eddy-covariance flux measurements of methane and nitrous oxide. Int. Agrophysics. https://doi.org/10.1515/intag-2017-0042.
Neubauer, S.C., 2014. On the challenges of modeling the net radiative forcing of wetlands: reconsidering Mitsch et al. 2013. Landscape Ecol. 29, 571–577. https://doi.org/10.1007/s10980-014-9986-1.
Nisbet, E.G., Dlugokencky, E.J., Manning, M.R., Lowry, D., Fisher, R.E., France, J.L., Michel, S.E., Miller, J.B., White, J.W.C., Vaughn, B., Bousquet, P., Pyle, J.A., Warwick, N.J., Cain, M., Brownlow, R., Zazzeri, G., Lanoisellé, M., Manning, A.C., Gloor, E., Worthy, D.E.J., Brunke, E., Labuschagne, C., Wolff, E.W., Ganesan, A.L., 2016. Global Biogeochemical Cycles 1–15. https://doi.org/10.1002/2016GB005406. Received.
Nisbet, E.G., Manning, M.R., Dlugokencky, E.J., Fisher, R.E., Lowry, D., Michel, S.E., Myhre, C.L., Platt, S.M., Allen, G., Bousquet, P., Brownlow, R., Cain, M., France, J.L., Hermansen, O., Hossaini, R., Jones, A.E., Levin, I., Manning, A.C., Myhre, G., Pyle, J.A., Vaughn, B.H., Warwick, N.J., White, J.W.C., 2019. Very strong atmospheric methane growth in the 4 years 2014–2017: implications for the Paris Agreement. Glob. Biogeochem. Cycl. 33, 318–342.
Novick, K.A., Ficklin, D.L., Stoy, P.C., Williams, C.A., Bohrer, G., Oishi, A.C., Papuga, S.A., Blanken, P.D., Noormets, A., Sulman, B.N., Scott, R.L., Wang, L., Phillips, R.P., 2016. The increasing importance of atmospheric demand for ecosystem water and carbon fluxes. Nat. Clim. Chang. https://doi.org/10.1038/nclimate3114.
Olson, D., Griffis, T.J., Noormets, A., Kolka, R., Chen, J., 2013. Interannual, seasonal, and retrospective analysis of the methane and carbon dioxide budgets of a temperate peatland. J. Geophsyical Res. - Biogeosciences 118, 226–238. https://doi.org/10.1002/jgrg.20031.
ORNL DAAC, 2018. Fixed Sites Subsetting and Visualization Tool. ORNL DAAC, Oak Ridge, Tennessee, USA Subset obtained for MCD15A2H product at site id 'pe_loreto_quistococha_forest_reserve' (Accessed 05 February 2020).
Otieno, D., Lindner, S., Muhr, J., Borken, W., 2012. Sensitivity of peatland herbaceous vegetation to vapor pressure deficit influences net ecosystem CO2 exchange. Wetlands. https://doi.org/10.1007/s13157-012-0322-8.
Page, S.E., Rieley, J.O., Banks, C.J., 2011. Global and regional importance of the tropical peatland carbon pool. Glob. Chang. Biol. https://doi.org/10.1111/j.1365-2486.2010.02279.x.
Pangala, S.R., Enrich-prast, A., Basso, L.S., Peixoto, R.B., Bastviken, D., Marotta, H., Silva, L., Calazans, B., Hornibrook, E.R.C., Luciana, V., 2017. Large emissions from floodplain trees close the Amazon methane budget. Nat. Publ. Gr. 552, 230–234. https://doi.org/10.1038/nature24639.
Papale, D., Reichstein, M., Aubinet, M., Canfora, E., Bernhofer, C., Kutsch, W., Longdoz, B., Rambal, S., Valentini, R., Vesala, T., Yakir, D., 2006. Towards a standardized processing of Net Ecosystem Exchange measured with eddy covariance technique: algorithms and uncertainty estimation. Biogeosciences 3, 571–583.
Ratcliffe, J., Andersen, R., Anderson, R., Newton, A., Campbell, D., Mauquoy, D., Payne, R., 2018. Contemporary carbon fluxes do not reflect the long-term carbon balance for an Atlantic blanket bog. Holocene. https://doi.org/10.1177/0959683617715689.
Reichstein, M., Falge, E., Baldocchi, D., Papale, D., Aubinet, M., Berbigier, P., Bernhofer, C., Buchmann, N., Gilmanov, T., Granier, A., Grünwald, T., Havránková, K., Ilvesniemi, H., Janous, D., Knohl, A., Laurila, T., Lohila, A., Loustau, D., Matteucci, G., Meyers, T., Miglietta, F., Ourcival, J.M., Pumpanen, J., Rambal, S., Rotenberg, E., Sanz, M., Tenhunen, J., Seufert, G., Vaccari, F., Vesala, T., Yakir, D., Valentini, R., 2005. On the separation of net ecosystem exchange into assimilation and ecosystem respiration: Review and improved algorithm. Glob. Chang. Biol. https://doi.org/10.1111/j.1365-2486.2005.001002.x.
Restrepo-Coupe, N., da Rocha, H.R., Hutyra, L.R., da Araujo, A.C., Borma, L.S., Christoffersen, B., Cabral, O.M.R., de Camargo, P.B., Cardoso, F.L., da Costa, A.C.L., Fitzjarrald, D.R., Goulden, M.L., Kruijt, B., Maia, J.M.F., Malhi, Y.S., Manzi, A.O., Miller, S.D., Nobre, A.D., von Randow, C., Sá, L.D.A., Sakai, R.K., Tota, J., Wofsy, S.C., Zanchi, F.B., Saleska, S.R., 2013. What drives the seasonality of photosynthesis

across the Amazon basin? A cross-site analysis of eddy flux tower measurements from the Brasil flux network. Agric. For. Meteorol. https://doi.org/10.1016/j.agrformet.2013.04.031.

Roucoux, K.H., Lawson, I.T., Jones, T.D., Baker, T.R., Coronado, E.N.H., Gosling, W.D., Lähteenoja, O., 2013. Vegetation development in an Amazonian peatland. Palaeogeogr. Palaeoclimatol. Palaeoecol. 374, 242–255. https://doi.org/10.1016/j.palaeo.2013.01.023.

Sabbatini, S., Mammarella, I., Arriga, N., Fratini, G., Graf, A., Hörtnagl, L., Ibrom, A., Longdoz, B., Mauder, M., Merbold, L., Metzger, S., Montagnani, L., Pitacco, A., Rebmann, C., Sedlák, P., Šigut, L., Vitale, D., Papale, D., 2018. Eddy covariance raw data processing for CO 2 and energy fluxes calculation at ICOS ecosystem stations. Int. Agrophysics. https://doi.org/10.1515/intag-2017-0043.

Saleska, S.R., Miller, S.D., Matross, D.M., Goulden, M.L., Wofsy, S.C., Da Rocha, H.R., De Camargo, P.B., Crill, P., Daube, B.C., De Freitas, H.C., Hutyra, L., Keller, M., Kirchhoff, V., Menton, M., Munger, J.W., Pyle, E.H., Rice, A.H., Silva, H., 2003. Carbon in Amazon forests: unexpected seasonal fluxes and disturbance-induced Losses. Science. https://doi.org/10.1126/science.1091165.

Saleska, S.R., Wu, J., Guan, K., Araujo, A.C., Huete, A., Nobre, A.D., Restrepo-Coupe, N., 2016. Dry-season greening of Amazon forests. Nature. https://doi.org/10.1038/nature16457.

Salo, J., Kalliola, R., Häkkinen, I., Mäkinen, Y., Niemelä, P., Puhakka, M., Coley, P.D., 1986. River dynamics and the diversity of Amazon lowland forest. Nature. https://doi.org/10.1038/322254a0.

Saunois, M., Bousquet, P., Poulter, B., Peregon, A., Ciais, P., Canadell, J.G., Dlugokencky, E.J., Etiope, G., Bastviken, D., Houweling, S., Janssens-Maenhout, G., Tubiello, F.N., Castaldi, S., Jackson, R.B., Alexe, M., Arora, V.K., Beerling, D.J., Bergamaschi, P., Blake, D.R., Brailsford, G., Bruhwiler, L., Crevoisier, C., Crill, P., Covey, K., Frankenberg, C., Gedney, N., Höglund-Isaksson, L., Ishizawa, M., Ito, A., Joos, F., Kim, H.S., Kleinen, T., Krummel, P., Lamarque, J.F., Langenfelds, R., Locatelli, R., Machida, T., Maksyutov, S., Melton, J.R., Morino, I., Naik, V., O'Doherty, S., Parmentier, F.J.W., Patra, P.K., Peng, C., Peng, S., Peters, G.P., Pison, I., Prinn, R., Ramonet, M., Riley, W.J., Saito, M., Santini, M., Schroeder, R., Simpson, I.J., Spahni, R., Takizawa, A., Thornton, B.F., Tian, H., Tohjima, Y., Viovy, N., Voulgarakis, A., Weiss, R., Wilton, D.J., Wiltshire, A., Worthy, D., Wunch, D., Xu, X., Yoshida, Y., Zhang, B., Zhang, Z., Zhu, Q., 2017. Variability and quasi-decadal changes in the methane budget over the period 2000-2012. Atmos. Chem. Phys. https://doi.org/10.5194/acp-17-11135-2017.

Saunois, M., Stavert, A.R., Poulter, B., Bousquet, P., Canadell, J.G., Jackson, R.B., Raymond, P.A., Dlugokencky, E.J., Houweling, S., Patra, P.K., Ciais, P., Arora, V.K., Bastviken, D., Bergamaschi, P., Blake, D.R., Brailsford, G., Bruhwiler, L., Carlson, K.M., Carrol, M., Castaldi, S., Chandra, N., Crevoisier, C., Crill, P.M., Covey, K., Curry, C.L., Etiope, G., Frankenberg, C., Gedney, N., Hegglin, M.I., Höglund-Isakson, L., Hugelius, G., Ishizawa, M., Ito, A., Janssens-Maenhout, G., Jensen, K.M., Joos, F., Kleinen, T., Krummel, P.B., Langenfelds, R.L., Laruelle, G.G., Liu, L., Machida, T., Maksyutov, S., McDonald, K.C., McNorton, J., Miller, P.A., Melton, J.R., Morino, I., Müller, J., Murgia-Flores, F., Naik, V., Niwa, Y., Noce, S., O'Doherty, S., Parker, R.J., Peng, C., Peng, S., Peters, G.P., Prigent, C., Prinn, R., Ramonet, M., Regnier, P., Riley, W.J., Rosentreter, J.A., Segers, A., Simpson, I.J., Shi, H., Smith, S.J., Steele, P.L., Thornton, B.F., Tian, H., Tohjima, Y., Tubiello, F.N., Tsuruta, A., Viovy, N., Voulgarakis, A., Weber, T.S., van Weele, M., van der Werf, G.R., Weiss, R.F., Worthy, D., Wunch, D., Yin, Y., Yoshida, Y., Zhang, W., Zhang, Z., Zhao, Y., Zheng, B., Zhu, Qing, Zhu, Qiuan, Zhuang, Q., 2020. The Global Methane Budget 2000–2017. Earth Syst. Sci. Data 12, 1561–1623. https://doi.org/10.5194/essd-2019-128.

Schaefer, H., Fletcher, S.E.M., Veidt, C., Lassey, K.R., Brailsford, G.W., Bromley, T.M., Dlugokencky, E.J., Michel, S.E., Miller, J.B., Levin, I., Lowe, D.C., Martin, R.J., Vaughn, B.H., White, J.W.C., 2016. A 21st-century shift from fossil-fuel to biogenic methane emissions indicated by13CH4. Science. https://doi.org/10.1126/science.aad2705.

Shuttleworth, W.J., Gash, J.H.C., Lloyd, C.R., Moore, C.J., Roberts, J., Filho, A.D.O.M., Fisch, G., De Paula Silva Filho, V., Ribeiro, M.D.N.G., Molion, L.C.B., De Abreu Sá, L.D., Nobre, J.C.A., Cabral, O.M.R., Patel, S.R., Carvalho De Moraes, J., 1984. Eddy correlation measurements of energy partition for Amazonian forest. Q. J. R. Meteorol. Soc. https://doi.org/10.1002/qj.49711046622.

Smith, M.N., Stark, S.C., Taylor, T.C., Ferreira, M.L., de Oliveira, E., Restrepo-Coupe, N., Chen, S., Woodcock, T., dos Santos, D.B., Alves, L.F., Figueira, M., de Camargo, P.B., de Oliveira, R.C., Aragão, L.E.O.C., Falk, D.A., McMahon, S.M., Huxman, T.E., Saleska, S.R., 2019. Seasonal and drought-related changes in leaf area profiles depend on height and light environment in an Amazon forest. New Phytol 222, 1284–1297. https://doi.org/10.1111/nph.15726.

Tanner, C. B. and Thurtell, G. W., 1969, Anemoclinometer Measurements of Reynolds Stress and Heat Transport in the Atmospheric Surface Layer, Research and Development Technical Report, ECOM 66-G22-F, Final Report.

Stoy, P.C., Mauder, M., Foken, T., Marcolla, B., Boegh, E., Ibrom, A., Arain, M.A., Arneth, A., Aurela, M., Bernhofer, C., Cescatti, A., Dellwik, E., Duce, P., Gianelle, D., van Gorsel, E., Kiely, G., Knohl, A., Margolis, H., Mccaughey, H., Merbold, L., Montagnani, L., Papale, D., Reichstein, M., Saunders, M., Serrano-Ortiz, P., Sottocornola, M., Spano, D., Vaccari, F., Varlagin, A., 2013. A data-driven analysis of energy balance closure across FLUXNET research sites: The role of landscape scale heterogeneity. Agric. For. Meteorol. https://doi.org/10.1016/j.agrformet.2012.11.004.

Tang, A.C.I., Stoy, P.C., Hirata, R., Musin, K.K., Aeries, E.B., Wenceslaus, J., Melling, L., 2018. Eddy Covariance Measurements of Methane Flux at a Tropical Peat Forest in Sarawak, Malaysian Borneo. Geophys. Res. Lett. https://doi.org/10.1029/2017GL076457.

Taylor, M.A., Celis, G., Ledman, J.D., Bracho, R., Schuur, E.A.G., 2018. Methane Efflux Measured by Eddy Covariance in Alaskan Upland Tundra Undergoing Permafrost Degradation. J. Geophys. Res. Biogeosci. https://doi.org/10.1029/2018JG004444.

van Lent, J., Hergoualc'h, K., Verchot, L., Oenema, O., van Groenigen, J.W., 2019. Greenhouse gas emissions along a peat swamp forest degradation gradient in the Peruvian Amazon: soil moisture and palm roots effects. Mitig. Adapt. Strateg. Glob. Chang. https://doi.org/10.1007/s11027-018-9796-x.

Vourlitis, G.L., Filho, N.P., Hayashi, M.M.S., de, S., Nogueira, J., Caseiro, F.T., Campelo, J.H., 2002. Seasonal variations in the evapotranspiration of a transitional tropical forest of Mato Grosso, Brazil. Water Resour. Res. https://doi.org/10.1029/2000wr000122.

Wang, S., Zhuang, Q., Lähteenoja, O., Draper, F.C., Cadillo-Quiroz, H., 2018. Potential shift from a carbon sink to a source in Amazonian peatlands under a changing climate. Proc. Natl. Acad. Sci. U. S. A. https://doi.org/10.1073/pnas.1801317115.

Webb, E.K., Pearman, G.I., Leuning, R., 1980. Correction of flux measurements for density effects due to heat and water vapour transfer. Q. J. R. Meteorol. Soc. https://doi.org/10.1002/qj.49710644707.

Wille, C., Kutzbach, L., Sachs, T., Wagner, D., Pfeiffer, E.M., 2008. Methane emission from Siberian arctic polygonal tundra: Eddy covariance measurements and modeling. Glob. Chang. Biol. https://doi.org/10.1111/j.1365-2486.2008.01586.x.

Wilson, K., Goldstein, A., Falge, E., Aubinet, M., Baldocchi, D., Berbigier, P., Bernhofer, C., Ceulemans, R., Dolman, H., Field, C., Grelle, A., Ibrom, A., Law, B.E., Kowalski, A., Meyers, T., Moncrieff, J., Monson, R., Oechel, W., Tenhunen, J., Valentini, R., Verma, S., 2002. Energy balance closure at FLUXNET sites. Agric. For. Meteorol. 113, 223–243.

Wong, G.X., Hirata, R., Hirano, T., Kiew, F., Aeries, E.B., Musin, K.K., Waili, J.W., Lo, K.S., Melling, L., 2018. Micrometeorological measurement of methane flux above a tropical peat swamp forest. Agric. For. Meteorol. https://doi.org/10.1016/j.agrformet.2018.03.025.

Wood, J.D., Griffis, T.J., Baker, J.M., Frankenberg, C., Verma, M., Yuen, K., 2017. Multiscale analyses reveal robust relationships between gross primary production and solar induced fluorescence. Geophys. Res. Lett. 44, 533–541. https://doi.org/10.1002/2016GL070775.

Wutzler, T., Lucas-Moffat, A., Migliavacca, M., Knauer, J., Sickel, K., Šigut, L., Menzer, O., Reichstein, M., 2018. Basic and extensible post-processing of eddy covariance flux data with REddyProc. Biogeosciences. https://doi.org/10.5194/bg-15-5015-2018.

Young, D.M., Baird, A.J., Charman, D.J., Evans, C.D., Gallego-Sala, A.V., Gill, P.J., Hughes, P.D.M., Morris, P.J., Swindles, G.T., 2019. Misinterpreting carbon accumulation rates in records from near-surface peat. Sci. Rep. https://doi.org/10.1038/s41598-019-53879-8.